MODELING INTERACTIONS BETWEEN CELLS AND THE AQUEOUS ENVIRONMENT

BY

YICHEN HE

THESIS

Submitted in partial fulfillment of the requirements
for the degree of Master of Science in Environmental Engineering in Civil Engineering
in the Graduate College of the
University of Illinois at Urbana-Champaign, 2015

Urbana, Illinois

Adviser:

Professor Rosa M. Espinosa-Marzal

ABSTRACT

When nanoparticles, heavy metals and ions generated from industry are released to the environment, they may react with cells of organisms and can be toxic to them. The primary purpose of this study is to develop a novel cell model that mimics several reveal cell properties including nanomechanical behavior, and to investigate the interactions between them and the aqueous environment. The novel cell model developed in this work has potential applications as a platform to investigate cytotoxicity.

In this study, the cell membrane model consists of a hydrogel-supported lipid-bilayer. Hydrogels are cross-linked polymer networks that can absorb large amounts of water without dissolving or loosing their shape (1). A number of hydrogels are stimuli-sensitive. They can change their structures and properties in response to changes in environment, such as pH (2), temperature (3), and ionic strength. These polymer hydrogels have wide applications in various biological and clinical fields (4), including drug delivery (5), contact lenses (6), and artificial implants (7). Biocompatibility and hydrophilic properties of hydrogels are the basis of these applications (8). In this study, neutral PAAm hydrogel is used as support for the lipid bilayer. The used hydrogel is a (neutral) polyacrylamide (PAAm) hydrogel. The lipid bilayer used in this study is Eggphosphatidycholine (EggPC). A layer-by-layer method with two polyelectrolytes, poly(sodium 4-styrenesulfonate) (PSS) and poly(allylamine hydrochloride) (PAH), was used to graft the EggPC to the neutral PAAm hydrogel. An electrostatic attraction is the main driving force for the adsorption of the bilayer on the hydrogel-supported polyelectrolyte multilayer (PEM). The developed cell model has been fully characterized in this work by using different surface analytic techniques.

On a silica substrate, lipid vesicle ruptures and fuses above a critical vesicle concentration to form a continuous lipid bilayer. QCM-D measurements and AFM imaging were performed to verify the formation of the bilayer on the silica substrate. The adsorption kinetics of the lipids on the hydrogel-supported PEM completely differs from that on the “hard” silica substrate. However, the change in dissipation supported the formation of a lipid bilayer. Further, the adsorbed mass on bovine serum albumin (BSA) verified that the adsorbed lipids on the PAAm hydrogel-PEM complex form a lipid bilayer, but the surface coverage is only partial. Thus, BSA adsorbs on the PEM through the defects of the lipid bilayer.

The interactions between cells and the environment happen through the cell membrane, and very often the nanomechanical behavior determines such interactions, and also cell sensing and response. In this work, the nanomechanical properties of PAAm hydrogels, PAAm-supported PEM and lipid bilayers were studied using atomic force microscopy (AFM), including both nano-indentation and the response to

shear. A significant difference in the elasticity (and viscoelasticity) between the behavior of the hydrogel-supported PEM and the silica-supported lipid bilayer was concluded from these studies, as well as very different mechanisms for the energy dissipation upon shear. The question that remains to be answered is the behavior of the cell model constituted of the hydrogel-supported PEM and the lipid bilayer, which is the outlook of this work.

ACKNOWLEDGMENTS

I would like to express my sincere gratitude to my advisor Professor Rosa Espinosa-Marzal for giving me the opportunity to be part of this project. This project would not have been possible without the continuous support she has given me. Her motivation, and enthusiasm inspired me all the time. Her patience and knowledge lead me through this project.

Besides my advisor, I would like to thank my colleagues in our research group—SIEN research group for all the support. Especially I would like to thank Andres Jurado and Prathima Nalam for helping me with AFM imaging. I would like to thank all the colleagues on 4th floor in Civil and Environmental Engineering department.

I would to express my appreciation to Scott MacLaren for training and help with AFM.

Last but not least, thanks to my parents, numerous friends, who always support and love me along the way.

TABLE OF CONTENTS

CHAPTER 1 INTRODUCTION

When nanoparticles, heavy metals, and other contaminants generated from industry are released to the environment, like water bodies, they may interact with living cells and can be toxic to them. The motivation for this study is to advance our fundamental understanding of the interactions between cell membranes and the environment. For that purpose, we have developed a novel cell model system that enables to mimic the properties of real cell membranes and to investigate the interactions between living cells and aqueous environment. This system will be applied to identify mechanisms of cytotoxicity in future works.

1.1 Model for Biological Membranes

Cell membranes are permeable biological membrane with high selectivity, which separates interior of living cells and outside environment. It maintains the required conditions for the interior cell environment by regulating the molecular transport across the membrane, while providing mechanical stability to the living cell. Cell membranes are dynamic structures that undergo changes as a response to the environment that depend on the stage within the cell lifecycle. In addition, cell membranes have a complex composition and microstructure, usually characterized by a phospholipid bilayer, with embedded proteins and lipopolysaccharides (9). Instead of using living cells, it is a common practice to employ biological membrane models for systematic investigations of particle-membrane interactions as this allows longer-term studies, and systematic investigations of several parameters. Natural or synthetic lipid bilayers are commonly used as models for cell membranes to study the effects of pollutants, such as metal ions, organics and surfactants, on membrane cytotoxicity (10). Usually the lipid bilayer is adsorbed onto a solid substrate (11). Some studies, however, have pointed out several limitations of this model. First of all, the high friction between the lipid bilayer and the solid substrate leads to a decreased lateral mobility of the lipid bilayer, in contrast to the 2D fluid nature of the membrane of living cells (12). Furthermore, since the investigated lipid bilayers are just a few nms in height, the proteins embedded into the lipid bilayer usually lack on mobility owing to their strong interaction with the substrate, which differs from the behavior of the proteins embedded in living cell membranes (13). Besides, the diffusion path for ions and other solutes in supported lipid bilayers is just 2-3 nm in height, which strongly differs from real cells.

To overcome or partially solve the limitations mentioned above, a (soft) polymer film has been inserted between the lipid bilayer and the solid substrate (14, 15). Thus, a thin polymer layer has been attached to the solid substrate, providing the polymer-supported lipid bilayer with long-lateral range mobility, which makes the membrane model more similar to real cell membranes. The polymer film acts as a spacer between the lipid bilayer and the solid substrate, not only to minimize the solid substrate

effects (stiffness), but it also provides a larger contact area for embedded proteins. In contrast to the short diffusion path length for the particles across the lipid bilayer-solid substrate model, this polymer-supported lipid matrix provides a longer diffusion path length, which includes both the lipid bilayer and the polymer.

Based on literature review, the use of a hydrophilic polymer as a soft support for the model membrane is still a relatively new but promising system (16,17). The investigated supports are polyelectrolyte multilayers and have a thickness of a few tens of nanometers, which is still small in comparison to real cells. In this project, a novel cell membrane model consisting of a hydrogel-supported lipid bilayer is used to study interactions between albumin and microparticles with cell membranes in aqueous environment. The height of the hydrogel can be tuned in the µm-range (4-200 µm). The polymer consists of polyacrylamide hydrogel (PAAm), and the lipid bilayer is Eggphosphatidycholine (EggPC), which is grafted to the hydrogel by a polyelectrolyte multilayer.

The pathway of cytotoxicity can be very different depending on the involved interactions. For example, studies have shown that direct contact between nanoparticles and cell membrane is necessary for cell damage (18); the adsorption of nanoparticles has still not been well understood. Cell-particle interactions are controlled by surface properties, surface forces and solution conditions.

Typical interactions between silica particles in water involve van der Waals (VDW), electrostatic double layer, and hydration forces (19). VDW forces result from quantum mechanical fluctuation of electrons, which induce a dipole moment in atoms leading to an attractive (Coulombic) force. The superposition of these interactions for the atoms at the solid surface constitutes the VDW force, which is usually a weak attractive force. The electrostatic double layer force arises from the surface charges on cells and particles in an aqueous system and the formation of a diffuse and Stern layer. The Derjaguin-Landau-Verwey-Overbeek (DLVO) theory considers the sum of attractive VDW and repulsive electrostatic double layer forces. Since most cell membranes have surface charges, electrostatic and VDW forces play an important role in the adsorption of macromolecules on cell membranes, in the interaction with other cells, and with nanoparticles (20). For example, as a result of the electrostatic repulsion, negatively charged nanoparticles are usually assumed to adsorb less to a cell membrane membrane than neutral and positively charged nanoparticles.

In contrast to this, negatively charged gold nanoparticles with citric acid stabilizing ligands are observed to adsorb to cell membrane (21). This phenomenon is explained by nonspecific adsorption of serum proteins onto the gold surface. These proteins induce the nanoparticles to enter into cells via the mechanism of receptor-mediated endocytosis. The endocytic fate has been observed with both gold and iron oxide nanoparticles (22, 23). As a matter of fact, in nature most molecules are internalized through endocytosis upon contact with the cell membrane. In addition, since the major component of cell

membranes – the phospholipid bilayer – is highly hydrophilic and undergoes dynamic fluctuations, repulsive hydration is believed to contribute to the interaction between nanoparticles and cell membranes as well (24). Besides the interaction forces mentioned above, the compliant and deformable membrane together with the cell heterogeneity because of surface embedded proteins and other structures further complicate the interactions between nanoparticles and cell membrane (25).

Protein adsorption occurs in both natural and man-made systems at interfaces. It has important implications in different fields, such as medical, environmental and biotechnological process, and therefore a fundamental understanding of how proteins adsorb to interfaces, including membrane cells, is necessary.

Proteins are composed of polypeptide units connected by amide linkages (26). Protein adsorption is a complicated process, which results from combination of different types of interaction with the adsorbent. However, independent on the mechanism for adsorption, adsorption occurs spontaneously if the overall Gibbs energy of the system decreases. The decrease in Gibbs energy can be achieved by decrease in the enthalpy and/or increase in the entropy (27). Factors that determine protein adsorption mainly include hydrophilicity of the surfaces, electrostatic interactions, hydrophobic interactions, and other effects including hydrogen bonding and dipolar interactions, as well as conformational entropy changes of proteins (27).

Most native globular proteins contain a secondary structure. These structures form when the proteins are stabilized by hydrogen bonds and by hydrophobic interaction between amino acid side groups. Proteins inherently fold into a secondary structure, which leads to an entropy loss. The introduction of an interface provides a region where protein can unfold without exposing the hydrophobic side. The structural change of protein reduces hydrophobic interactions, and thus reduces secondary structure formation. As a result, surface-adsorbed protein molecule involves a significant increase in conformational entropy (27).

As mentioned above, another factor influencing protein adsorption is the hydrophilicity of the surfaces. Some studies have shown that albumin adsorbs more significantly on hydrophobic surfaces (28, 29) than on hydrophilic surfaces, while other studies show opposite trends (30, 31). For example, human serum albumin (HSA) is shown to adsorb more onto the hydrocarbon chains than onto the polar groups of lipid layers (32). Hydration water can be retained between the adsorbed protein and the substrate when adsorption occurs on hydrophilic surfaces (27). Even though the results are contradictory, hydrophilicity is considered to strongly contribute to protein adsorption.

Electrostatic interactions strongly influence protein adsorption. In most of the cases, proteins and substrates are electrically charged and surrounded by counter ions when they are in aqueous environments. An electrical double layer forms at charged interfaces in aqueous medium. If the protein and the substrate

are (locally) oppositely charged, they attract each other and adsorption takes place. However, if only one, either the protein or the substrate, is charged or if they have same charge sign, proteins can still adsorb spontaneously. This phenomenon has been explained as a result of ion diffusion between solution and the adsorbed layer to counterbalance charges and to avoid charge accumulation in the adsorption sites (33, 34). Ion association and ion pair formation is expected to occur in this region. As a result, the electrostatic repulsion is decreased and protein adsorption is possible.

In this project, bovine serum albumin (BSA) is used to investigate the protein adsorption onto our model cell membrane. BSA is the most abundant serum protein and is described as a soft protein (29), which shows a high affinity for surfaces. BSA can adsorb at hydrophilic surfaces under conditions of electrostatic repulsion (27).

Living cells are capable of sensing mechanical forces and respond to them (35). Cells can change mechanical properties based on the substrate they are cultured on. For instance, the stiffness of cell decreases when grown on a soft substrate (36,37). The mechanical response of cells has been increasingly recognized as a major regulator of several cellular processes. For example, studies have shown that cell mechanics partially govern differentiation of cells (38,39). It is also believed that if cells are in contact with nanoparticles, the mechanical properties of cells can change. It has been proved that contact with MgO particles contribute to mechanical damage of the cell membranes (40).

The mechanical properties of cells determine the extent of cell deformation. Distinct mechanical properties have been measured for different cells. The relation between specific cells and their mechanical properties is a promising medical application to differentiate healthy cells and cancer cells (41,42). The measurement of the elastic moduli of cells is widely used as an indicator of cellular changes. These findings indicate that mechanical signals and properties are essential in the process of cell processes, sensing and response to external stimuli (43). As a result, understanding the mechanical properties of cells is becoming increasingly important. However, compared to the understanding level of chemical-induced cell signals, cell sensing and response to mechanical forces remain a relative new area of research that needs more study.

A variety of methods have been applied successfully to measure the mechanical properties of a single cell, including optical traps (44), atomic force microscopy (AFM) (45), and microplate cell manipulation (46), etc. Among these techniques, AFM is the mostly employed technique over the past decade to quantitatively measure cell's stiffness due to its incomparable precision and high spatial resolution. AFM has been used to measure the elasticity of a wide range of different cell types, such as cancer cells (47), and stem cells (48).

For elastic materials, the measured stiffness is independent of the deformation rate, whereas for viscoelastic materials, the measured stiffness is strongly dependent on the deformation rate. It has been

shown that at low indentation depth, cells show almost an ideal elastic response, while at large indentation depths the cell stiffness is dependent on the loading rate. When higher forces are applied, viscous effects will increasingly contribute to the measured cell stiffness (49,50). In literature, cell stiffness has a large variation, however, most studies agree that cells respond stiffer when probed at higher loading rate (49), as it is common for (viscoelastic) gels. Most of the experiments show that the cell stiffness obeys a weak power law as a function of speed (44,51). In this project, AFM is used to measure the stiffness of cell models and to characterize viscoelastic behavior and response to shear forces.

CHAPTER 2 MATERIALS AND METHODS

2.1 Materials

To prepare polyacrylamide (PAAm) hydrogel, 40% (w/v) acrylamide (AAm) stock solution (Sigma-Aldrich) and 2% (w/v) bis-acrylamide (Bis-AAm) stock solution (Sigma-Aldrich) were used as received. 0.1M NaOH, 3-Aminopropyltriethoxysilane (APES) and 0.5% (v/v) glutaraldehyde in phosphate-buffered saline (PBS) were used to pretreat the 25-mm circular coverslips. Dichlorodimethylsilane (DCDMS) was used to pretreat the 25 × 75-mm glass slides. Tetramethylethylenediamine (TEMED) and 10% (w/v) ammonium persulfate (APS) were used as accelerator and initiator of the reaction, respectively. Distilled H_2O was used for these solutions. Other materials include hot plate, 6-well plate, 35-mm petri dishes, Kimwipes, and vacuum desiccator.

To prepare the charged PAAm hydrogels, itaconic acid (Sigma-Aldrich), AAm, Bis-AAm, and APS (Sigma-Aldrich) were used without further purification. Distilled H_2O was used for all solutions. A hot plate was needed to provide heat for the polymerization.

To prepare the lipid vesicles, a suspension of egg phosphatidylcholine (EggPC) 1 mg/ml in chlololform (Avanti) was used as received. Milli-Q water (Milli-Q, 18.2MΩ, Millipore, USA) was used for all solutions. A mixture of 10 mM Tris, pH 8.0 and 100 mM NaCl was used as buffer.

For the polyelectrolyte multilayer, poly(sodium 4-styrenesulfonate) solution (PSS, 70 kDa), poly(allylamine hydrochloride) (PAH, 17.5 kDa) and sodium chloride were obtained from Sigma and used as received. Milli-Q water (Milli-Q, 18.2MΩ, Millipore, USA) was used for all polymer, buffers and salt solutions. Unless indicated, water means Milli-Q water.

2.2 Synthesis of PAAm hydrogels

By adjusting the concentration of the monomer, AAm, and the cross-linker, Bis-AAm, stiffness of acrylamide hydrogel can be easily modified. To mimic the elasticity of living cells, which varies between 100Pa to 100kPa, the selected concentrations of the different chemicals is shown in Table 1. This composition gives a Young's Modulus of ~2.8kPa based on AFM results.

Table 1. Composition of polyacrylamide hydrogel

	AAm mol/L H_2O	Bis-AAm mol/L H_2O	IA mol/L H_2O	APS mol/L H_2O	TEMED mol/L H_2O
PAAm	1.407	0.002	0	0.0044	0.0067
PAAm-co-IA	1.4	0.016	0.146	0.1675	0
PAAm-co-IA	1.4	0.016	0.055	0.1675	0

PAAm hydrogels were prepared according to the protocol given by Tse et al. (52). 25-mm coverslips were placed on a hot plate and 500μL of 0.1 M NaOH was added to each coverslip so that the solution covers the entire coverslip. The coverslips with solution were heated to 80℃ until the liquid was evaporated. Boiling of solution was avoided. After evaporation, a thin semi-transparent film of NaOH remained on the coverslip. If the film was not uniform, NaOH was diluted by adding 500 μL of distilled H_2O to the coverslip and heated until the film of NaOH was uniform. Coverslips were then placed in the fume hood and 200 μL of APES was added to the surface of each coverslip. After 5 min of reaction, both the top and bottom of coverslipswere rinsed under distilled H_2O to remove excess APES. Coverslip was immersed in a petri dish with distilled H_2O twice, each time for 5 min. After rinsing twice with distilled H_2O, the coverslip was immersed in0.5% (v/v) glutaraldehyde in phosphate-buffered saline into a petri dish for 30 min. Coverslips were wiped with a Kimwipe and further dried by blowing nitrogen on them. The pretreated coverslips remained viable for 48h. DCDMS was spread onto both sides of 25 × 75-mm glass slides in the fume hood. After 5 min, excess DCDMS was removed with a Kimwipe. Each glass slide was rinsed under distilled H_2O for 1 min.

Acrylamide and bis-acrylamide were mixed at the ratio given in Table 1 in distilled H_2O. The mixture was degassed under strong vacuum for 15 min to remove the dissolved oxygen. 1/100 total volume of APS and 1/1000 total volume of TEMED were added to the mixture. The solution was vortexed for about 30 seconds. 25μL gel solution was pipetted onto the glass slide and the solution was sandwiched between glass slide and coverslip with its treated side facing down. The gel was allowed to polymerize for 10 min. The bottom glass slides were removed and the coverslips were rinsed with distilled H_2O to remove unpolymerized acrylamide. The coverslips were placed in a 6-well plate in distilled H_2O with the gel coated side face up and stored at 4℃. Hydrogels can be stored for one month without changes in the mechanical properties. In this project, hydrogel were stored for a maximum of 15 days. This protocol was followed to prepare the hydrogels for AFM studies.

To prepare the hydrogels on TInAS sensors, only the steps with NaOH and glutaraldehyde were skipped to avoid staining of the sensors that would affect the optical path. Hydrogels were also prepared on QCM gold sensors, but the steps with NaOH, APES and glutaraldehyde were skipped as it was found to improve the quality of the grafting to the gold sensor. The amount of polymer solution pipetted on TInAS sensors was 0.75 μL and 0.5 μL on QCM sensors, which lead to a hydrogel thickness of 6 μm and 4 μm respectively.

2.3 Synthesis of PAAm-co-IA hydrogels

Even though polymer hydrogels has broad applications in various areas, many potentials uses are limited by their low mechanical strength (53). The interpenetrating polymer network (IPN) technique is a

possible way to improve the mechanical behavior of hydrogels. IPNs are formed when two or more cross-linked polymer networks co-exist and at least one is cross-linked in the presence of the other (54). In this study, semi-interpenetrating hydrogel networks based on polyacrylamide and itaconic acid was also used. Itaconic acid introduces negative charges to the hydrogel so that a polyanionic hydrogel is obtained. Swelling behavior, and mechanical properties can differ from the neutral hydrogel. By adjusting the amount of cross-linker and amount of monomer, the mechanical properties of PAAm-co-Itaconic acid (PAAm-co-IA) hydrogels can be altered. To achieve a similar elastic modulus to that of the neutral hydrogels (~2 kPa) a higher crosslinking concentration (Bis-AAm) was required (see Table 1).

PAAm-co-IA hydrogels were prepared according to the protocol given by Bera et al. (55) and Kayaman et al. (8). AAm, itaconic acid, MBA and APS were dissolved in water separately and then mixed. The same protocol was used to treat the 25-mm coverslips and 25 × 75-mm glass slides as for the neutral hydrogel. Upon mixture, a 25μL droplet of polymer solution was pipetted on the glass slide and covered by a coverslip to make the "sandwich", and then placed on a hot plate at 70℃ for 30 min to 1hr to polymerize. The time needed to fully polymerize depends on the copolymer composition. After polymerization, patterns appeared around the edge of sensor.

2.4 Lipid Vesicle

2.4.1 Preparation of Lipid Vesicles

Small unilamellar vesicles (SUVs) were prepared according to the protocol given by Keller et al. (56). 10mg EggPC in chloroform was transferred to a round bottom flask. The lipid mixture was dried onto the walls of a continuously rolled round bottom flask under vacuum and left for 3-4 hours to ensure complete removal of solvents. 10mL buffer (10 mM Tris buffer pH 8.0, 100 mM NaCl) was added to the round bottom flask. Nitrogen gas was blown to the flask to avoid lipid contact with oxygen. The dried lipid was resuspended in buffer by vortexing for 30 min. Lipid vesicles were formed by sonicating the suspension to clarity using 1/8" microtip of Branson probe sonicator. The sonication was carried out on ice in 5s pulses separated by 5s cooling period. The total sonication time initially was 60 min. Due to aging of the probe sonicator, the sonication time was increased to 90 min. The vesicle suspension was spun at 150,000 × g for 4.5 h in an ultracentrifuge to separate SUVs from large lipid structures. Based on the protocol(58), after ultracentrifuge, the supernatant above the pellet should be drawn off in three fractions and the middle fraction should be used for adsorption experiments. However, in our experiments only 2 fractions formed every time, and the upper fraction was used and characterized by Dynamic Light Scattering. The SUV fractions were stored under N_2 in small vials at 4℃.

2.5 Dynamic light scattering (DLS)

After preparation of the lipid vesicles, the solution was diluted to a concentration of 0.1 mg/ml in Tris buffer pH 8.0 10 mM, 100 mM NaCl, to be consistent with the concentration used for all adsorption experiments. Both, size and zeta potential of lipid vesicles were measured. The refractive index and light absorption were assumed to be 1.47 and 0.1, respectively. For both size and zeta potential measurement, three runs were taken, and average and standard calculation were determined.

2.6 Swelling experiments

The swelling ratio of the PAAm hydrogel was measured in all solutions used in the experiments, including water, 1 mM hepes, 10 mM hepes, 10 mM Tris buffer pH 8.0 with 100 mM NaCl, and 500 mM NaCl. 2mL hydrogel solution was polymerized inside of 4cm diameter petri dish instead of on top of a coverslip to prepare 15 hydrogels, with 3 replicates for each solution. After preparation, hydrogels were rinsed with DI water and then dried on a hot plate at 80℃. After the hydrogels were completely dry, they were weighed on a balance and the mass of each piece was recorded. The completely dried PAAm hydrogels were then immersed in the selected solutions in separate petri dishes (10 cm diameter). The weight of the hydrogel immersed in solution was measured with time until equilibrium was achieved.

2.7 Quartz crystal microbalance (QCM)

The gold QCM sensor was cleaned according to the following procedure: exposure to UV ozone for 10 min, immersion into a 1:1:5 solution of hydrogen peroxide (30%), ammonia hydroxide (25%) and water heated to 75℃ for 5 min, immediately rinsed with water and dried with nitrogen, and a final exposure to UV ozone for 10 min. The silica QCM sensors were cleaned by exposure to UV ozone for 10 min, sonicated in sodium dodecyl sulfate (SDS) solution (2% w/v) for 30 min, immediately rinsed with water, dried with nitrogen and exposure to UV ozone for 10 min. QCM crystals were used immediately after cleaning. Before each experiment, the fluid cell was cleaned by running SDS (2% w/v) for at least 10 min and then water for at least 30 min and air to dry the tubing with a flow rate of 300μL/min. The fluid cell was further dried in N_2 flow.

2.7.1 Formation of Polyelectrolyte Multilayers (PEM) on PAAm hydrogels

Two polyelectrolytes, PAH 2mg/ml in water, and PSS, 2mg/mL in water with NaCl (500 mM) were prepared and sonicated at 50℃ overnight to fully dissolve the polymers. Right before use, the polyelectrolyte solutions were filter using a 0.2μm nylon sterile syringe filter.

PAAm hydrogels were made ex situ on gold sensors as described above. After equilibrating with water for at least 1 h, the system was tuned to the resonant frequency of the hydrogel on the gold sensor. Water was flowing through the cell for another 10 min to obtain a baseline. During the measurement, first

NaCl solution (500 mM) was introduced to the system. Then, the PAAm gel was coated by alternating adsorption of aqueous solutions of PAH (2mg/mL) and PSS (2mg/mL). In this project, two PEM systems, $(PSS\text{-}PAH)_2$ and PAH-$(PSS\text{-}PAH)_2$were investigated as discussed in the Results and Discussion section. Each polyelectrolyte was allowed to adsorb for at least 15 min or till equilibrium with a $50\mu L$/min flow rate. Between adsorption of each layer, PAAm hydrogel was rinsed with water for at least 10 min or till equilibrium, to wash away weakly adsorbed polyelectrolytes.

2.7.2 Vesicle adsorption and lipid bilayer formation

Adsorption of lipid bilayers adsorption was tested on three different systems: directly on hard substrates (silica and gold), on PEM directly adsorbed onto the gold QCM sensor, and on PAAm-supported PEMs (also called PAAm-PEM complexes).

Lipid vesicle adsorption on gold and silica sensors was performed as it follows. After cleaning, QCM silica and gold sensors were equilibrated with Tris buffer pH 8.0 (10 mM) and NaCl (100 mM). After equilibration, the system was tuned to the resonant frequency of the crystals. Tris buffer pH 8.0 (10 mM) and NaCl (100 mM) was run for another 10 min to get a baseline in buffer. Then buffer was replaced by lipid vesicle diluted in buffer to a concentration of 0.1 mg/ml. After reaching equilibrium, lipid vesicle solution was replaced with buffer to wash away weakly adsorbed lipid vesicles. These were our reference measurements to compare to vesicle adsorption on the polymer films and hydrogels.

As lipid vesicles did not adsorb on PAAm and PAAm-co- IA hydrogels, hydrogels were coated by a layer-by-layer approach with four to five layers, with PAH as the top layer. The results on PAAm-co-IA hydrogels were not successful owing to failures of grafting the charged hydrogel to gold, and therefore the Results Section focuses on the results obtained for PAAm. After the last rinsing with water, Tris buffer pH 8.0 (10 mM) with NaCl (100 mM) and $CaCl_2$ (0-25 μM) was flowed through the cell. After reaching equilibrium, adsorption of lipid vesicles diluted to 0.1 mg/ml in Tris buffer pH 8.0 (10 mM) with NaCl (100 mM) and $CaCl_2$ ($0 - 25\mu M$) took place. In contrast to the direct adsorption on ahard substrate, $CaCl_2$ was added to enhance the adsorption of lipid vesicle. Lipid vesicle adsorption was also investigated on gold-supported PEM, i.e. in absence of PAAm hydrogel following the same protocol.

2.7.3 Bovine Serum Albumin (BSA) Adsorption

In order to understand the adsorption mechanisms of albumin on hydrogel-supported lipid bilayers, six different systems were investigated and compared. The first system was albumin adsorption on silica-supported lipid bilayer. The protocol for lipid vesicle adsorption on QCM sensors was described above. After lipid bilayer formation, the Tris buffer pH 8.0 (10 mM), and NaCl (100 mM) was replaced by hepes (10 mM) to get a baseline. The second system was albumin adsorption after lipid adsorption on silica-supported PAH-$(PSS\text{-}PAH)_2$. The protocols for the PEM formation and lipid vesicle adsorption

were described in section 2.7.2. Albumin adsorption was also investigated on PEM-hydrogel complexes (hydrogel-supported PEM) after lipid adsorption. In addition, albumin adsorption was investigated on hydrogel-supported PEM without previous lipid adsorption and in neutral and charged PAAm hydrogels. In all six systems, after equilibrium was achieved in Hepes (10 mM), hepes was replaced by BSA (1 mg/ml) in hepes to investigate albumin adsorption, and finally rinsed with hepes to remove weakly adsorbed albumin.

2.8 Transmission Interference Adsorption Sensor (TInAS)

A novel high-speed adsorption sensor based on thin-film interferometry at interfaces called Transmission Interference Adsorption Sensor (TInAS) was used as a standalone instrument in this project to measure the optical thickness of adlayers. The basic TInAS setup includes a flow cell, which is built on the top of the sensor surface and a tubing system connected to the flow cell. The TInAS sensors used in this project composed of a flat glass substrate with a 25nm aluminum layer (mirror) and 2-3um silica layer (spacer) on top of each other in the presenting order. Usually the adsorption reaction occurs on top of the silica. However, in this project, a thin layer about $6\mu m$ of hydrogel was grafted to the sensor ex-situ as described in the Experimental Section and the sorption experiments were performed on the hydrogel. The hydrogel is porous and the solute can diffuse into the pores; therefore not only adsorption but also absorption takes place, which can more broadly be called "sorption". We will here still refer to this phenomenon as adsorption for simplicity. A detailed discussion on theory and experimental setup for TInAS can be found in Heuberger et al.'s article (57).

Before each measurement, TInAs sensors were sonicated in toluene, isopropanol, and ethanol, each for 10 min, dried with nitrogen and exposed to UV ozone for 15 min to clean. The other components of the cell were sonicated in ethanol for 10 min before use.

2.8.1 Formation of Lipid Bilayer on TInAs sensor

The procedure of lipid vesicle adsorption on TInAs sensor was similar to the procedure for QCM. After cleaning, TInAs sensors were equilibrated with Tris buffer pH 8.0 (10 mM) and NaCl (10 mM) while the thickness of spacer was measured in buffer at the same time. When the sensor was equilibrated with the buffer, the thickness of spacer was entered manually into the software. The buffer was allowed to flow for another 10 min to obtain the baseline. After equilibration, the buffer was replaced by the lipid vesicles solution at a a concentration of 0.1 mg/mL. The refractive index of the lipids was assumed to be 1.42. After reaching equilibrium, the cell was rinsed with buffer to wash away weakly adsorbed lipid vesicles. The flow rate was 230 μL/min.

2.8.2 Formation of Polyelectrolyte Multilayers (PEM) on PAAm hydrogel

PAAm hydrogel was grafted on a TInAs sensor first and then allowed to equilibrate in water. The thickness of hydrogel was adjusted manually in the software to bring the thickness of adlayer to zero before adsorption takes place. The refractive index of PAAm gel and polyelectrolyte were assumed to be 1.35 and 1.42, respectively. The refractive index of solvent was assumed to be 1.337. After a 10 min baseline in water, the PEM was deposited on the PAAm hydrogel by alternating adsorption of aqueous solutions of PAH (2mg/mL) and PSS (2mg/mL). Both the four layer system $(PSS\text{-}PAH)_2$ and the five layer $PAH\text{-}(PSS\text{-}PAH)_2$ were deposited on PAAm hydrogels for comparison. Each polyelectrolyte was allowed to adsorb at least for 15 min or till equilibrium with a $230\mu L$/min flow rate. Between adsorption of each layer, hydrogel was rinsed with water for at least 10 min or till equilibrium to wash away the weakly adsorbed polyelectrolyte.

2.8.3 Bovine Serum Albumin (BSA) Adsorption

The refractive index of PAAm hydrogels and BSA were assumed to be equal to 1.35 and 1.42, respectively. First the PAAm hydrogel was allowed to equilibrate with hepes (10 mM). The thickness of hydrogel was adjusted manually in the software to bring the thickness of adlayer to zero before adsorption takes place. Hepes (10 mM) was allowed to run for another 10 min to get a baseline. Then BSA (1 mg/mL) in hepes (10 mM) was injected into the cell and allowed to adsorb. After the adsorption reached equilibrium, hepes (10 mM) was injected into the cell to remove weakly adsorbed BSA.

2.8.4 Collapsing and Swelling of PAAm gels

Two sets of experiments were carried out with either water or hepes (10 mM). After BSA adsorption, either in water or in hepes, a high concentration of C_aCl_2 solution 1M in water (hepes (10 mM)) was flowed through the flow cell. TInAS only measures the dry mass or optical thickness of the adsorbate, and the thickness of hydrogel is assumed to remain constant as there is no desorption of polymer. However, since the optical path is highly related to the refractive index of the adsorbate layer, and this changes as hydrogel swells or collapses, it is possible to measure swelling and collapse of gels. Finally, the hydrogel was rinsed with water (hepes) again. The flow rate was kept constant through the adsorption experiment, which equals to $230\mu L/min$. The temperature was room temperature throughout the experiment.

2.9 Fourier Transform Infrared Spectroscopy (FTIR)

The IR spectrum of PAAm hydrogel, and PAAm-IA hydrogels was measured using FTIR-ATR within the range 400 cm^{-1} to 4000 cm^{-1}. Both PAAm and PAAm-IA hydrogels were made as described above, except that the hydrogels were synthesized in a 4 cm diameter petri dish instead of a coverslip. A

small piece of PAAm hydrogel was cut from the large piece with a spatula. A background run was performed with a droplet of DI water covering the window. Since hydrogels were composed mostly of water, scanning water as background effectively excluded the influence of water.

The IR spectrum of PAAm hydrogel with PAH-(PSS-PAH)$_2$, and PAAm hydrogel with PAH-(PSS-PAH)$_2$ and lipid bilayer was also obtained. Here it is important to investigate the surface of the gel, so, a different method was used. First, PAAm hydrogels were synthesized on coverslips as described before. The cover slips with the hydrogels were immersed in PAH (2mg/mL) and PSS (2 mg/mL) solutions with 500 mM NaCl in a 4cm diameter petri dish, each for 15 min. After each cycle of adsorption, the PAAm hydrogel was rinsed with water twice to remove the weakly adsorbed polyelectrolyte before the next polyelectrolyte solution was added. After the PEM formation, some of the samples were also immersed in Tris buffer pH 8.0 (10 mM) with NaCl (100 mM) and $CaCl_2$ (25 μM) for 30 min. Then the PAAm hydrogel was immersed in lipid vesicle solution with a concentration of 1 mg/mL with $CaCl_2$ (25 μM) for 2 hours to allow adsorption. Here a longer time and higher concentration of adsorption was used compared to the QCM experiments, to compensate the lack of flow in the immersion experiments. After the adsorption, the PAAm hydrogel was immersed again in Tris buffer pH 8.0 (10 mM) with NaCl (100 mM) and $CaCl_2$ (25 μM) for 30 min to remove the nonadsorbed lipid vesicles. The coverslip with the prepared samples was placed on top of the ATR crystal with the PAAm hydrogel facing down.

2.10 Atomic Force microscopy

AFM indentation and friction experiments on PAAm hydrogels were carried out with a MFP-3D (Asylum Research). Indentation with conventional sharp AFM tips results in a high local stress on the hydrogel, which likely induces damage. Measurement using sharp pyramidal tips is usually 2 to 3 times higher than the spherical tips (58). In this project, a colloidal sphere with a 10μm diameter was glued to the end of the cantilever. Under this condition, the force is distributed over a large area, and the damage can be considered negligible. Indentation measurements and lateral force measurements were performed on various hydrogel systems, and lipid bilayers.

2.10.1 Nanoindentation

After calibration of the tipless cantilever to determine the normal spring constant by the thermal noise method, a colloidal sphere around 10 μm in diameter was glued to the tip of the cantilever (59). The sensitivity of the cantilever was determined in a normal force measurement on a glass slide immersed in water every time before measurements.

After PAAm hydrogel was grafted on the coverslip, the coverslip was fixed at the center of the lid of a 4 cm petri dish with an adhesive pad. A few droplets of water were deposited on the top of the hydrogel to avoid drying in air. Contact mode was used for nanoindentation. Since the adhesion was very

high, a 5μm force distance was used to pull out the colloid sphere after each indentation. The maximum loads were 20nN and 40nN, and the approaching speeds 0.1 $\mu m/s$, 0.5 $\mu m/s$, 2 $\mu m/s$, 10 $\mu m/s$, 30 $\mu m/s$ and 50 $\mu m/s$. For each speed, 10 successive normal forces were taken at each spot and three different spots indented per gel. The elastic modulus was determined from the force-distance curve upon approach by using Hertz contact model (60).

2.10.2 Lateral force measurements

A cantilever from the same box as the one used for friction measurements was used for lateral calibration. After determination of its normal spring constant, a 40 μm in diameter sphere was glued at the tip of the cantilever. The sphere was used to hit the edge of a clean silicon wafer at five different positions. The slope of the each curve was determined to determine the lateral spring constant according to the test probe method (61).

Load-dependent and speed-dependent friction forces were measured. Since the selected PAAm hydrogels are relatively soft, the contact area upon applied normal load was very large (calculated with the Herzian model for each load – for 5nN, it is ~4μm). In order to assure the lateral movement of the colloid sphere, the maximum force was 5nN, and the minimum sliding distance was 7.5 μm.

For the friction vs. load experiments, a sliding distance of 15 μm was used to ensure the lateral motion. The scanning rate was set at 0.1 Hz, which lead to a sliding speed equal to 3 $\mu m/s$. The load was varied from 0.5nN to 5nN in increments of 0.5nN; the average and standard deviations were calculated from 10 friction loops at each load. The cantilever was withdrawn between each load.

For the friction vs. scanning speed measurements, a normal load of 5nN was maintained constant. The scanning rate was again set to be 0.1 Hz and the sliding distance varied from 5 μm to 50 μm, which lead to a sliding speed from 1 $\mu m/s$ to 15 $\mu m/s$.

CHAPTER 3 RESULTS AND DISCUSSION

All experiments were performed on freshly prepared gels as aging was found to increase the stiffness of the hydrogels, in agreement with previous reports.

3.1 DLS measurements

The phospholipid used in these investigations was Eggphosphatidylcholine (Egg-PC, 1,2-Diacyl-*sn*-glycero-3-phosphocholine, or 3-*sn*-Phosphatidylcholine) and the vesicles were prepared according to the described method. The vesicles have a size of 35.2 ± 3.8 nm, and a zeta potential of -5.8 ± 0.9 mV in the selected buffer (10 mM Tris pH 8, 100 mM NaCl) with a vesicle concentration of 0.1 mg/ml.

3.2 Swelling ratio of the hydrogels in different solvents

The swelling ratio of the hydrogels was determined in various solutions. Figure 1 shows the swelling ratio calculated by:

$$SR = \frac{M_{wet} - M_{dry}}{M_{dry}}$$

where M_{dry} is the dry mass of the hydrogel (determined at 80ºC) and M_{wet} is the equilibrium weight of the hydrogel during water uptake.

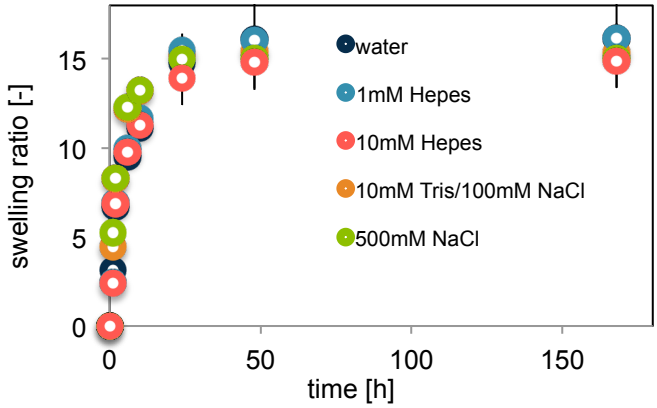

Figure 1: Swelling ratio of PAAm in pure water, 1 mM and 10 mM Hepes, 500 mM NaCl and Tris buffer as a function of time.

Figure 1 shows the negligible influence of the ionic strength in the range of ~0 mM (in Milli-Q water) to 500 mM (NaCl), and of pH (5.8 in nanopure, 7.1 in hepes and 8 in tris buffer), consistent with the non-charged properties of the polyacrylamide hydrogel. An equilibrium swelling ratio of ~14.1±2.6 is achieved after water uptake for 24h and the average swelling ratio for all solvents is 14.4±1.8 [-]. The variability between hydrogels is thus larger than between the results obtained at different ionic strengths and pH. The swelling ratio is smaller than that reported in (62) which can rely in the different protocol for the hydrogel synthesis. The values can be also underestimated as the gels are wet-dried before weighting.

3.3 Formation of PEM on neutral hydrogels: $(PSS\text{-}PAH)_2$ and $PAH\text{-}(PSS\text{-}PAH)_2$

The formation of the PEM on the neutral gel was monitored by QCM-D (see representative results in Figure 2). In our studies, the hydrogels were prepared ex situ on gold QCM sensors, and the baseline was determined with the hydrogel in water. Thus, the hydrogel represents the "substrate" for the further investigation of the formation of the PEM. The hydrogel is porous, and polymer diffusion into the pores is possible; further, the hydrogel-polyelectrolyte complexes can collapse and swell as a response to changes in ionic strength. The reason is that polyelectrolyte that remains within the hydrogel converts PAAm into a "charged" hydrogel, and therefore it makes it responsive to gradients in osmotic pressure. It has been previously shown that hydrogels can also become thermo-and pH-responsive when altered by layer-by-layer assembly of polyelectrolytes (63,64).

Besides, as a result of absorption the baseline can also change during the experiments, as described below. Such changes of the substrate do not occur on the classical QCM sensors, since they are rigid and non-porous (gold, quartz, silica). Representative QCM results for the PEM formation of $(PSS\text{-}PAH)_2$ on the PAAm hydrogel are shown in Figure 2.

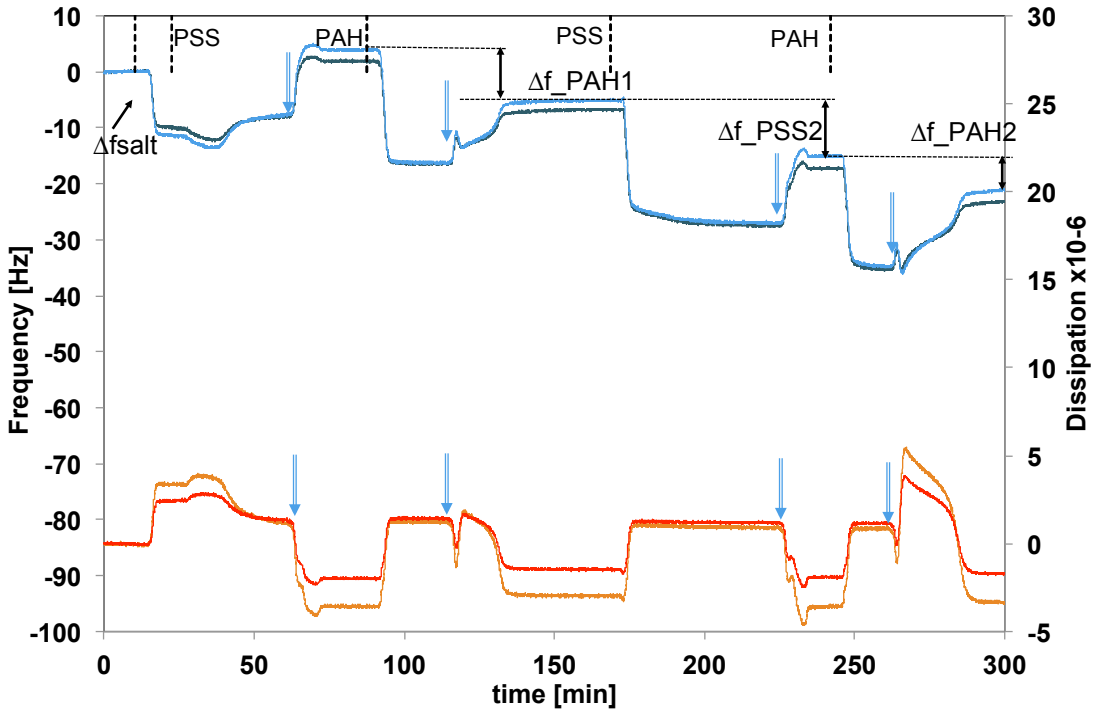

Figure 2:QCM-D data (frequency and dissipationx10^6) during PEM formation using NaCl solution (500 mM) before flowing the 1st polymer solution (PSS). Overtones 7th and 9th are shown. The dotted lines give the time at which the solution is changed; it takes 2-3 minutes for the solution to enter the chamber. The arrows point at the rinsing steps with water (single line black) after each layer deposition.

In the QCM measurements a solution of NaCl (500 mM) was first introduced into the cell and then the polymer solution, in deviation with the classical protocol for the layer-by-layer formation. This enables to distinguish between the influence of the density of the salty polymer solution and the adsorption of polymer on the changes in frequency and dissipation. The higher density and viscosity of the 500 mM NaCl solution compared to water (baseline) leads to the initial decrease in frequency (Δfsalt~-10Hz for the 7th overtone). Figure 2 also shows that the dissipation becomes negative after the 1st PSS adsorption (ΔD7~-2 for the 7th overtone). The negative dissipation is explained by the sorption of polymer within the porous hydrogel (63-66) –the pore size is expected to be ~100 nm (67), which increases the stiffness of the porous substrate. As a distinction between the absorption within the pores and at the hydrogel/solution interfaces is not possible, the new baseline cannot be determined.

During rinsing with water (blue arrows) the frequency increases and the dissipation decreases as a result of following concerted effects: i) decrease in density and viscosity of the solution - as the polymer solution with NaCl is exchanged by water (Δf_{salt}~-9.8±2 Hz for the 7th overtone), ii) swelling of the hydrogel – as it is effectively charged after polyelectrolyte absorption-, and iii) polymer desorption as the interactions between polyacrylamide and PSS have been shown to be weak (68). The overall changes during rinsing suggests that desorption of polymer and decrease in density of the solution are dominant.

The dissipation changes upon adsorption and desorption of the 2nd, 3rd and 4th layers is complex as well but most likely not related to the hydrogel support: It has been shown in microgel particles (63-66, 69,70) that only the 1st layer penetrates into the gel, although we cannot exclude that some weak absorption is taking place. Upon adsorption, we expect the polyelectrolyte to adsorb with the conformation in bulk and later to collapse at the surface; the change of conformation is associated with a change in frequency and dissipation. Upon rinsing with water, the frequency first increases owing to the decrease in density of the solution and then it slowly increases which can be related to desorption of weakly adsorbed polymer. The changes in dissipation upon rinsing with water are significant for PAH, which can be related to a rearrangement of the polymer chains to optimize interactions with the lower layers. Complex changes were also observed for the silica-supported PEM (see supplementary information) and they have been previously reported for another system (71).

Figure 3 summarizes the results obtained for PAH-(PSS-PAH)$_2$ with qualitatively similar results for the frequency and the dissipation. The negative dissipation suggests that the porous substrate also becomes stiffer upon absorption. The changes in frequency and dissipation indicate the successful formation of the PEM (see figure 4 for average values of frequency and dissipation for each layer) under the investigated conditions. In all cases upon rinsing with water the change in frequency increases (it become less negative); the increase is larger than expected for the change in density/viscosity, which suggests a significant swelling of the polymer-hydrogel complexes is not taking place.

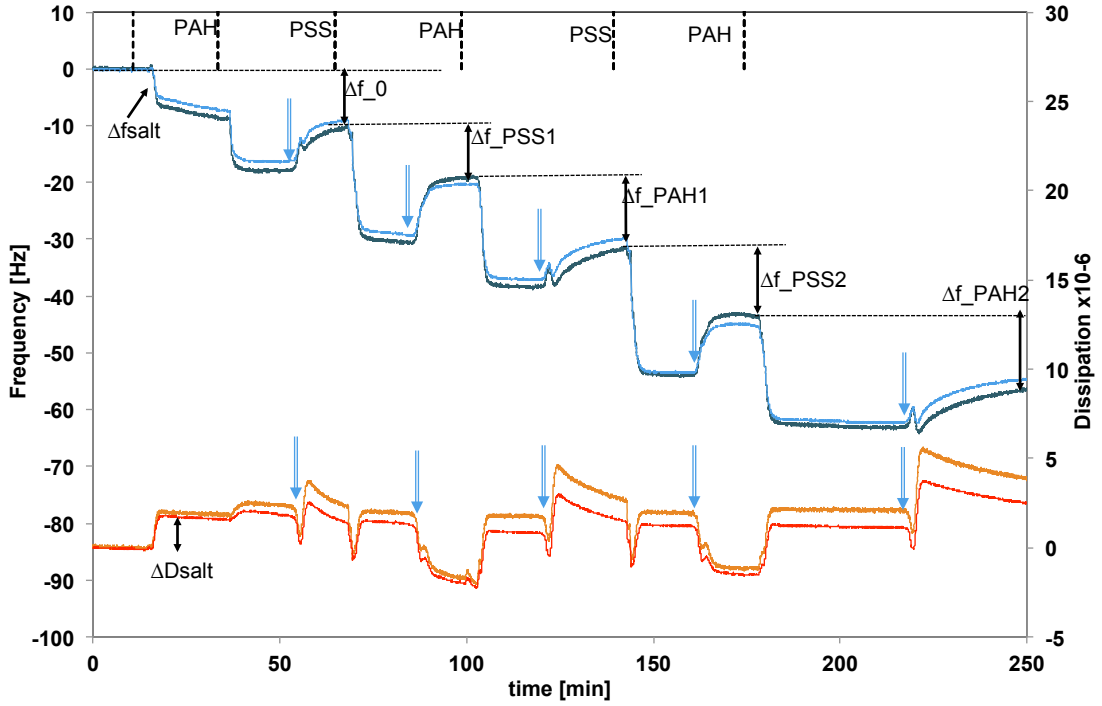

Figure 3: QCM-D data of frequency and dissipationx10^6 (7^{th} and 9^{th} overtones) during PEM formation on PAAm hydrogel rinsing with NaCl solution (500 mM) before flowing polymer solution. The dotted lines give the time at which the solution is changed; it takes 2-3 minutes for the solution to enter the chamber. The blue arrows point at the rinsing steps with water after each layer deposition. The changes in frequency for each layer are shown (with respect to the baseline in water).

Figure 4 shows a collection of the changes in dissipation and in frequency during the formation of each PE layer for the two investigated hydrogel-supported PEM. For PAH-$(PSS\text{-}PAH)_2$ (see dotted lines) a positive change in dissipation results upon PSS adsorption (PSS-1 and PSS-2) suggesting an increase in rigidity of the system, whereas the opposite effect is observed upon addition of PAH, which has a smaller MW. The corresponding negative change in frequency demonstrates the successful layer-by-layer formation. All values of frequency and dissipation changes were obtained with respect to the baseline in water. For $(PSS\text{-}PAH)_2$ (empty symbols), the positive frequency change results from the *absorption* of PSS-1 into the hydrogel (~3 Hz) while the negative dissipation supports the substrate is becoming stiffer ($\Delta D \sim -3 \times 10^{-6}$); the changes are small though (see arrows). For the following layers, the negative change in frequency accompanied by very small dissipation changes (0-1), supports the successful formation of this PEM on the hydrogel as well. The significant standard deviations are attributed to slightly different thicknesses of the gels and crosslinking degrees. The obtained values are similar to those measured for other PEM on a rigid and non-porous substrate (71), with the dissipation being smaller than ~4 $\times 10^{-6}$.

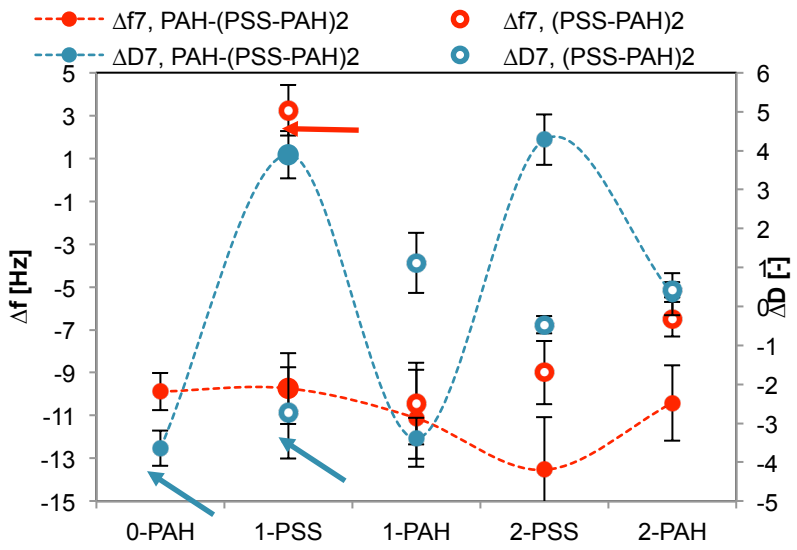

Figure 4: Changes in frequency and dissipation during PEM formation for each single layer in (PSS-PAH)2 (empty circles) and PAH-(PSS-PAH)2 (full circles).

PEM are usually soft or viscoelastic in nature due to the hydration water present in the film, and therefore the Sauerbrey expression often becomes invalid. For viscoelastic films, the mass can be deduced using the Voigt model (72), which assumes that the film has uniform thickness and density. However, absorption within the hydrogel substrate complicates the modeling, as the Voigt model cannot be used to model negative dissipation values. Instead, the dry mass of the PEM on the hydrogel can be determined by TInAS without the need of models or approximations. The interferometric technique measures the optical thickness $\boldsymbol{T}$ if the refractive index is known, which is directly proportional to the dry adsorbed mass given by $\boldsymbol{M_{dry}} = \frac{\boldsymbol{T(n_{adl}-n_{solv})}}{\boldsymbol{dn/dc}}$ (73).

Thus, this interferometric measurement is not sensitive to the water content. At the beginning of the experiment the optical thickness of the hydrogel was measured ($\boldsymbol{T_0}$~~187±9 from 10 measurements); this is used as baseline in the TInAS experiments ($\boldsymbol{T}$=0). The refractive index of PAAm is assumed to remain constant and equal to 1.35 [-]; a refractive index of 1.42 was assumed for the layer-by-layer and 1.337 for the solvent.

Figure 5 shows representative results for the two hydrogel-supported PEMs. It is to note that during the initial PSS adsorption, the optical thickness of $(PSS\text{-}PAH)_2$ becomes negative and equal to -0.772 nm, which is attributed to a hydrogel collapse. Collapse and swelling of hydrogels were also investigated in a separate series of experiments (not shown) with polyanionic hydrogels (PAAm co-polymers with itaconic acid) by TInAS It was demonstrates that upon increase in ionic strength of the

solution a negative optical thickness was measured during collapse ($T<T_0$), and the original thickness was recovered after re-equilibrating (swelling) the polyanionic in water ($T=T_0$). Although the loss of water cannot be detected by TInAS, the increase of refractive index is reflected in a shift of the interference fringes, i.e. of the optical path Tn (74). Since the refractive index is assumed to remain constant during the measurement, T decreases, although the dry mass remains constant.

Thus, when PSS diffuses into the hydrogel, the latter becomes effectively charged. The hydrogel is still hydrated by pure water, whereas the solvent is a NaCl solution with a concentration of 500 mM and PSS concentration of 1 mg/ml. Thus, the gradient in osmotic pressure is responsible for the gel collapse, while there is simultaneous PSS ab- and adsorption. As in our measurements, the baseline ($T = 0$) is set before polymer adsorption, T becomes negative upon initial gel collapse. Further investigations of the collapse and swelling behavior of the hydrogels after albumin sorption are discussed in the Supplementary Information in more detail.

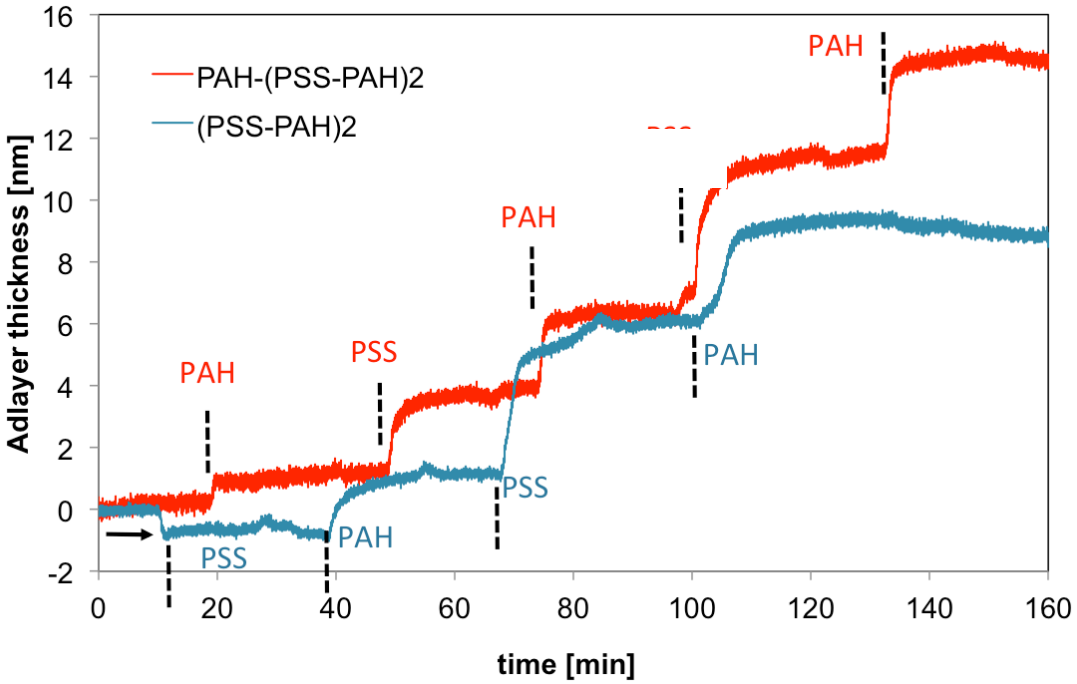

Figure 5: Optical thickness of the PEM adlayer for $(PSS\text{-}PAH)_2$(in blue) and PAH-$(PSS\text{-}PAH)_2$(in red)measured by TInAS.

Contrasting results were obtained for PAH-$(PSS\text{-}PAH)_2$. Here, the optical thickness T did not become negative upon PAH sorption, although the increase in $T$is much smaller than during the following steps. Thus, it cannot be excluded that absorption of the 1st PAH layer is also accompanied by hydrogelcollapse, although the increase in dry mass is dominant in this case. For the $(PSS\text{-}PAH)_2$, the final optical thickness of the PEM layer is T~ 8-9 nm, whereas T~14 nm is obtained form PAH-$(PSS\text{-}PAH)_2$. It is to note that during rinsing there is only a slight decrease of the optical thickness, which

suggests that no polymer desorption occurs. Hence, the changes in frequency and dissipation upon rinsing with water in QCM experimentsmust be related to both,decrease in salt concentration and rearrangement of the polymer chains (and loss of water).

3.4 Lipid bilayer formation

Reference adsorption measurements by QCM-D showed that the lipid vesicles adsorb on silica – where vesicle fusion takes place to form a lipid bilayer (figure 6, insets) –, and on gold (as vesicles, see SI), in agreement with ref. (75)**.** The thickness was calculated with the Voigt model assuming a density of the lipid bilayer equal to 1.5 g/cm3. No adsorption of lipid vesicles was detected on PAAm hydrogels, which demonstrates a weak interaction between vesicles and hydrated PAAm. On the polyelectrolyte multilayer (PEM) grafted to PAAm hydrogel –with PAH (positively charged) as top layer– vesicle adsorption took place but the kinetics of adsorption was completely different (figure 6). Vesicle adsorption was also studied on PAH-$(PSS\text{-}PAH)_2$ directly adsorbed onto a silica substrate for comparison, and the results are shown in the supplementary information.

On the silica substrates, it is well accepted that the vesicles first adsorb and then they fuse and form the bilayer (see also figure 7 with an AFM image or reference (76)). Vesicle fusion is typically dominated by surface adhesion energy between vesicles and the substrate as the adhesion enhances stress and leads to vesicle rupture and spreading after a critical surface concentration of adsorbed vesicles has been achieved. This behavior leads to the characteristic increase in dissipation followed by a notable decrease as the water is released; the frequency follows the opposite behavior. The vesicles contain large amounts of water, which explains the large dissipation, whereas the lipid bilayer is a much stiffer system.

On the PEM-hydrogel complexes the frequency rapidly decreases (Δf_7~-26 Hz) and a small peak was observed in the dissipation. This suggests the immediate rupture of the vesicles at the surface, which keeps the dissipation low, in agreement to ref. (77). The total change id frequency was very similar to that measured on the flat silica-coated QCM sensors. However, we expect the PEM-fluid interface to be rough, which enhances the surface area compared to flat surfaces leading to larger changes in frequency and dissipation compared to those of flat QCM sensors. The thickness of the lipid bilayer obtained by the Voigt model is ~3.1 nm, whereas a smaller thickness of ~2.1 nm was obtained for the PEM-hydrogel complexes, which suggests only a partial coverage.

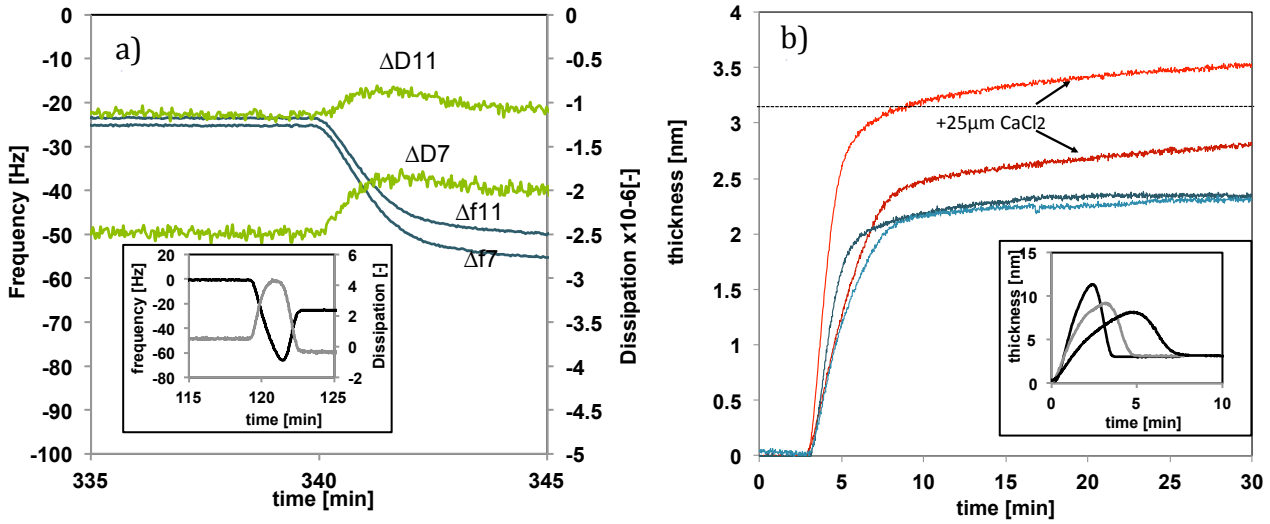

Figure 6: a) Characteristic change in frequency and dissipation (7th and 11thovertones) during lipid bilayer formation on PAAm hydrogels modified by PAH-(PSS-PAH)$_2$. The inset shows the Characteristic change in frequency and dissipation (7thovertone) on a silica substrate. B) Thickness of the lipid bilayer on four different altered hydrogels with PAH-(PSS-PAH)$_2$ calculated by the Sauerbrey equation, without addition of calcium (blue) and upon addition of calcium (red). The inset shows the thickness of the lipid bilayer on three different silica substrates calculated by the Voigt model.

It was also found that when PSS was used as top layer vesicle adsorption did not take place (not shown here), which supports the driving force for the adsorption to be the electrostatic interaction between the amino group in the PAH and the phosphate ion. It has been previously shown that a complexation of the lipid layer with segments from the second last layer is possible (76,78) owing to entanglements between PAH and PSS chains. Thus, a relevant surface density of sulfates on the top layer is also possible for our system. In fact, the vesicle adsorption was strongly enhanced by adding small amounts of Ca^{2+} (25µM) to the vesicle solution (79). Thus, it is likely that the calcium ions interact with PSS chains close to the PEM-solution interface and act as bridging between the slightly negatively charged vesicles and the PEM grafted to the hydrogel. Our results in figure 6b show that the resulting thickness increased upon addition of calcium, demonstrating a larger surface coverage, although there were discrepancies between experiments. As the PEM-hydrogel complexes are expected to be rough, a higher adsorbed mass is expected which might explain the larger thickness in some of these experiments.

The successful formation of the lipid bilayer was also demonstrated by AFM imaging of the QCM sensors. The lipid bilayer fully covered the (flat) silica substrate (figure 7). A scratch test was

performed to show the height of the bilayer (~2.5 nm, not shown). AFM imaging will be performed in close future to demonstrate discontinuities of the lipid bilayer.

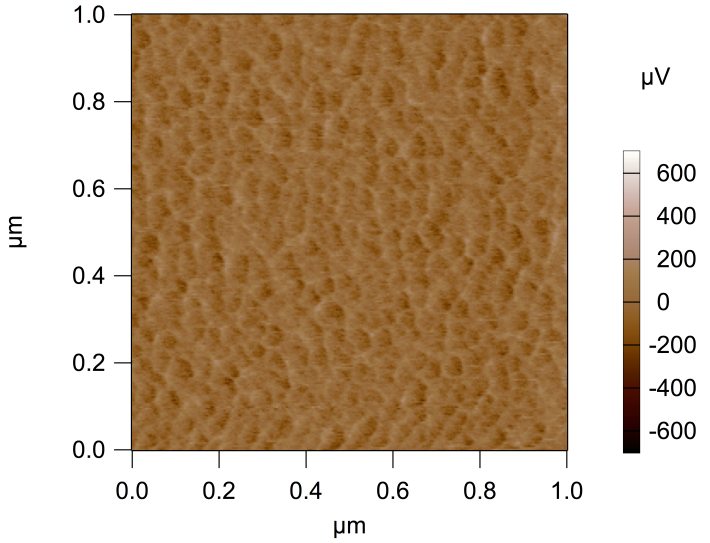

Figure 7: AFM image (lateral deflection) of the lipid bilayer a) on a silica substrate (QCM sensor). Scan rate = 0.75Hz, contact mode, sharp tip HQ: CSC38/No Al.

The adsorption of lipid vesicles was also measured by TInAS on rough silica substrates (the TInAS sensors) leading to an optical thickness of 4 nm; equilibrium was achieved within 5 minutes (dry mass=292 ng/cm^2 estimated with nadl=1.47 and dn/dc=0.182 g/cm3). As TInAS is not sensitive to the water content, the vesicle rupture cannot be detected, and only a continuous increase in thickness was observed to around 3.1 nm. AFM imaging in contact mode showed single vesicles adsorbed to the surface with a maximum number density of 10 per µm^2 (see supplementary information). The corresponding dry mass to this number density –estimated for vesicles with a diameter of 32 nm, phospholipid with a molar mass of 770 g/mol, and a surface area per phospholipid of 0.85 nm^2- is more than 2 orders of magnitude smaller than the dry mass measured by TInAS. This demonstrates that a larger amount of lipids was adsorbed in the TInAs experiment but it could not be detected by AFM imaging. As the roughness of the substrate is ~5.5 nm (RMS), i.e. larger than the lipid bilayer height, it is likely that the distinction of the lipid bilayer on the TInAS sensors is not possible by AFM and a (probably discontinuous) lipid bilayer along with single vesicles is present at the surface.

3.5 ATR-FTIR of the systems

Figure 8 (top) shows the IR spectrum of PAAm, of the PAAm-IA copolymer, and of the AAm and IA monomers. The amide group has three characteristic peaks (80): the first is at 1672 cm−1 (Amide I), representing the –C=O stretching vibration of the amide group. The second is at 1610 cm−1 (Amide II) and is primarily due to the –NH_2 bending vibration of the amide group and the third is the –CN stretching

vibration of the amide group at 1425 cm−1. The methylene backbone produces a characteristic peak at 1458 cm−1 due to the $–CH_2$ scissoring vibration. The shoulder at 1720 cm-1 and the peak at 1216 cm-1 are characteristic of the itaconic acid.

Fig. 8 (bottom) shows a section of the fingerprint region of the IR absorption spectrum for PAAm (black), PAAm-supported PAH-$(PSS\text{-}PAH)_2$, and adsorbed lipid onto the hydrogel-PEM complex ranging from 1750 cm-1 to 950 cm-1. The spectra of the pure phospholipid (published in ref. 66) can thus be used as a reference when comparing lipid spectra in the presence of the polyelectrolyte species.

The footprints of PSS are very pronounced in the spectrum of the hydrogel-PEM complex. Two characteristic peaks at 1178 cm-1 and 1125 cm-1 correspond to the asymmetric stretching vibrations of the S=O; the band at1037 cm-1 was assigned to the S=O symmetrical stretching vibrations, and the peak at 1008 cm-1 was attributed to aromatic in-plane vibrations (81). We clearly detect the peaks at 1037.5, 1009, 1127, and 1178 cm-1.

The identification of PAH is difficult. The band around 1500–1600 cm-1 is of the amide II and is attributed mainly to the distortion oscillations of N–H and the stretching oscillations of C–N while, the band around 1300 cm-1 of the amide III (82). The only peak that can be distinguished is at 1651 cm-1 (see arrow).

The presented section covers the phosphate region, including the asymmetric stretch of phosphate characterized by two components at ~1220cm-1 and ~1229 cm-1, as well as the symmetric stretch at ~ 1087 cm-1. The C–O–C carboxylic acid ester bond connecting the fattyacids to the glycerol contributes an asymmetric stretch vibration around 1183 cm-1 (a broad peak) and the symmetric C–O–C stretch is at 1065 cm-1. We detect the following peaks: 1178, 1086, 1065 and 1216 cm-1. The observed shifts of the peaks suggest interactions between the lipids and the polyelectrolytes, possibly owing to the interaction of PAH with the phosphate group of the lipid. According to ref (76). strong interaction of polyelectrolyte primary amino groups of PAH with phosphate can lead to phospholipid dehydration. The higher intensity of the peaks of the lipids indicates the presence of less water. Hence our results are consistent with a dehydration of the system.

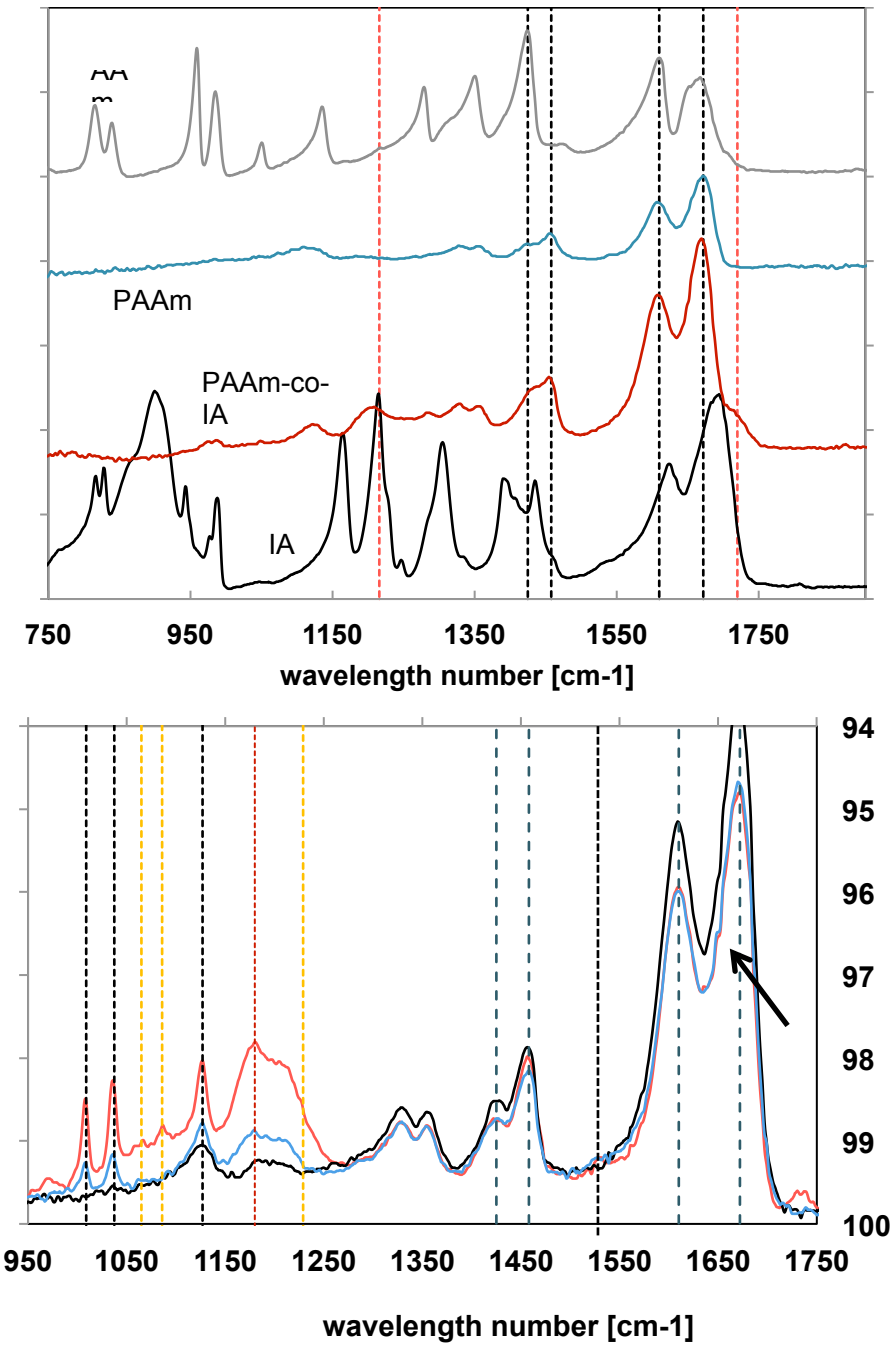

Figure 8: Top) IR spectra of IA and AAm monomers, and of the PAAm and PAAm-co-IA hydrogel. Bottom) FTIR-ATR spectra for PAAm (black), PAAm-supported PAH-(PSS-PAH)$_2$ (blue) and lipid on the hydrogel-supported PAH-(PSS-PAH)$_2$ (red). The lines give the peaks that have been used to identify the functional groups of the system components.

3.6 Adsorption studies of albumin on supported lipid bilayers

To understand the adsorption mechanisms of albumin on a lipid bilayer, various reference systems were investigated. Figure 9 shows representative results for the adsorption of lipid vesicles followed by albumin adsorption on (a) silica, and (b) PAH-(PSS-PAH)$_2$ directly adsorbed to silica. The Voigt model was used to model the results with a density of albumin assumed to be 1.32 g/cm3. The sorption of albumin in the hydrogel is shown in the supplementary information, and it completely differs.

Figure 9 shows the completely different adsorption kinetics of albumin on the compared substrates. Upon lipid bilayer formation on silica, the adsorption of albumin is strongly hindered; only a small increase in adlayer thickness is detected (adsorbed mass <80 ng/cm^2, <0.5 nm). Hydration repulsion possibility explains the hindered adsorption.

On silica-supported PEM, albumin adsorption is significant and the adlayer thickness is ~18 nm, i.e. it is smaller than the vesicle size. We first evaluate the vesicle adsorption: the characteristic well was also not observed (figure 22 in SI) which means that either the vesicles do not rupture at the interface, or the rupture is immediate after adsorption. The change in frequency is ~-90 Hz and that of the dissipation is ~2x10^{-6} and it remains constant. A simple calculation demonstrates that the measured change in frequency (~90 Hz) is smaller than the expected change for full coverage with vesicles: If one considers vesicles with 32 nm radius, a molar mass for the phospholipid equal to 770 g/mol and a surface area per phospholipid of ~0.85 nm^2, a full coverage of the QCM sensor with vesicles would lead to an adsorbed mass of 3.26 μg/cm2, or -184 Hz. This value includes the mass of water within the vesicle. Hence, the full coverage of the PEM-fluid interface with vesicles can be excluded. If the interface would be populated by vesicles, only a 50% of the surface area would be covered by vesicles.

Figure 10 shows the adsorption of vesicles and of albumin on various PEM-hydrogel complexes. In absence of vesicle adsorption, albumin adsorption is significant, as expected for PAH according to ref. (83): an average adlayer thickness of 30 nm of albumin is obtained by means of the Voigt model. We assume the results will be similar if the PEM is grafted directly to the silica substrate. On the PEM-adsorbed to silica, the albumin adlayer is only ~5 nm indicating the hindered adsorption of albumin by the lipids. As the reduction is much larger than ~50%, we thus conclude that vesicle rupture did take place on the silica-supported PEM. The silica-supported PEM is covered by a defective lipid bilayer, and albumin adsorbs in the defects. The larger thickness of the lipid bilayer (~18 nm) on the silica-supported PEM results from the significantly larger surface area of the PEM-hydrogel, i.e. to surface roughness. For rough substrates, there are more appropriate models than the Voigt mode, and therefore the modelling results are considered to be a rough estimation.

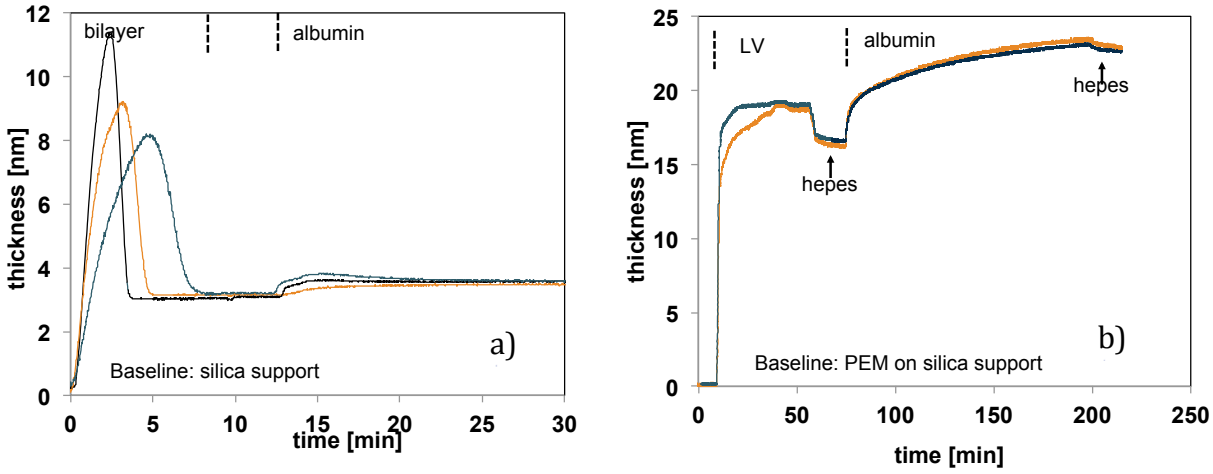

Figure 9: Thickness of the adlayer on a) a silica substrate and b) PAH-(PSS-PAH)2 calculated with the Voigt model. The first change in adlayer thickness occurs during vesicle adsorption, and the second change is caused by albumin adsorption.

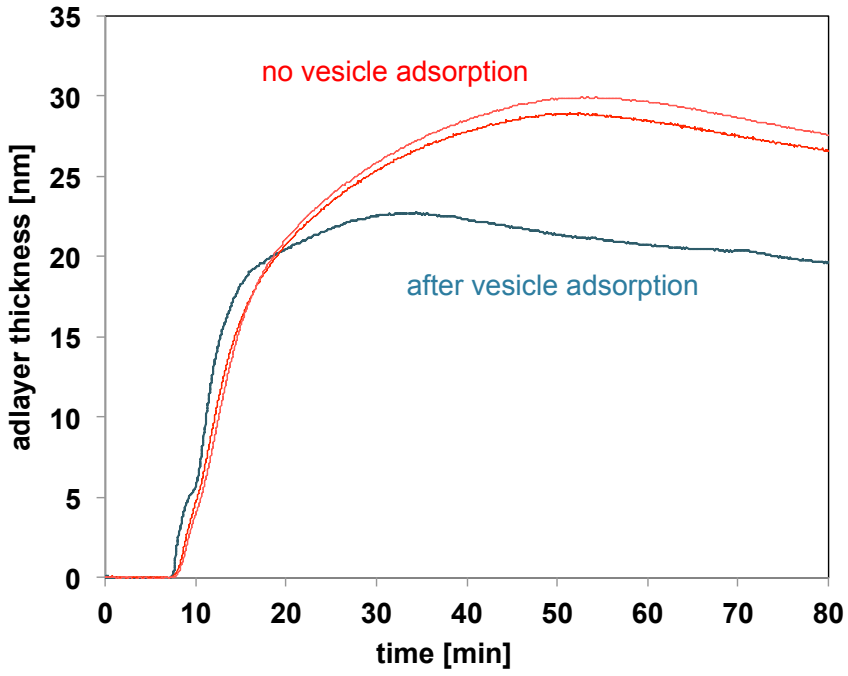

Figure 10: Adlayer thickness of albumin on PEM-hydrogel, and on a similar system after vesicle adsorption calculated by the Voigt model. The layer-by-layer formation and the adsorption of the vesicles are not shown in the diagram.

Finally, the thickness of the albumin adlayer on the hydrogel-supported PEM after vesicle adsorption is smaller than that in absence of lipids (figure 10). The reduction in albumin adsorption is, however, much smaller than on the silica-supported PEM, which suggests that the lipid bilayer, if it form,

has more defects. For attachment and rupture of the lipid vesicles, the affinity towards the support should be large enough – in our work through electrostatic interactions- whereas the formation of the continuous membrane requires local rearrangements of the lipid coverage, for which lateral mobility of the lipids along the surface of the support is an essential condition. It is possible that the mobility introduced by the hydrogel support enhances the lateral mobility of the vesicles so much that vesicle fusion is hindered, leading to a higher amount of defects. AFM imaging will be used to demonstrate the presence of the bilayer on the hydrogel-supported PEM. Future work will focus on mixtures of phosphatidylcholine and phosphatidylserine, as it has been shown to promote the lipid bilayer formation (76).

3.7 Nanoindentation by Colloidal Probe AFM

Sneddon's model (84) can be used to characterize the mechanical properties of viscoelastic polymers in AFM nanoindentation experiments provided certain conditions are fulfilled (85). Substrate effects need to be avoided by limiting the penetration depth to a maximum of 10% of the unperturbed film height. If $\delta << R$, the Sneddon model (86) for a rigid spherical indenter against a planar linear elastic material is equivalent to the well-known Hertz equation:

$$L = \frac{4}{3}\frac{E}{1-\nu^2}R^{0.5}\delta^{1.5}$$

where E and ν are the elastic modulus and the Poisson's ratio of the material (Poisson ratio = 0.45), respectively, and $E/(1-\nu^2)$ gives the reduced elastic modulus E_r. A better estimation of the contact geometry for very compliant materials, as hydrogels, is obtained by Segedin's approach (86) but this is outside the scope of the present study. Short-term viscoelasticity can be characterized through an indentation-rate-dependent reduced elastic modulus E_r (so-called effective elastic modulus) that is obtained from the force curve upon *loading*, during which E_r remains constant**.** By increasing the indentation rate, the viscoelastic effects are minimized. Under these conditions the force still scales with $\delta^{1.5}$as given by Eq. (1). Other power laws for the force as a function of the penetration depth are obtained depending on indenter geometry (84).

Nanoindentation experiments by colloidal Probe AFM on PAAm hydrogels and lipid bilayers were performed in water at different indentation rates between 0.1 µm s^{-1} and 50 µm s^{-1}. The maximum penetration depth δ_{max} was limited to 1% of the equilibrium hydrogel (~200 µm) to avoid substrate effects (85). Representative curves for PAAm in water are depicted in figure 11 at an indentation rate of 0.2 µm $s^{-1}$and 48 µm s^{-1}. The deformation is well described by the Hertz equation with a constant reduced elastic modulus for the whole indentation range of ~2 µm (regression correlation R^2>0.99). At least 20 successive compressions at three different spots on each hydrogel were indented at each speed. Hydrogels were less than 15 days old.

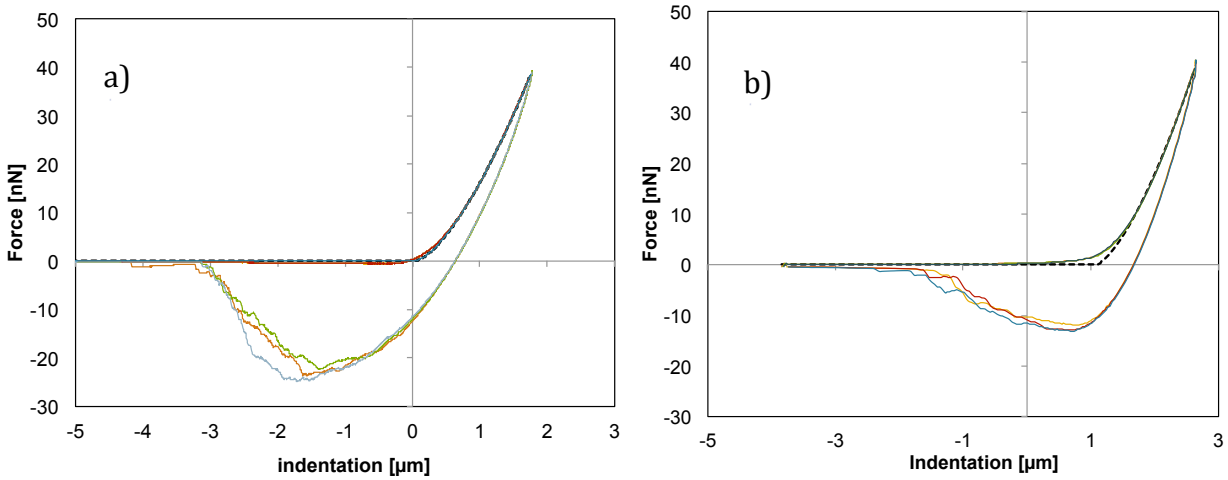

Figure 11: Indentation at a single position at a) 2 µm/s and b) 48 µm/s. The dotted line is the fitted Hertz model. Radius of the silica microsphere ~ 5 µm.

Figure12 shows the elastic moduli of neutral PAAm gels inwater as a function of the indentation rate (average values and standard deviations). The increase in elastic modulus with indentation speed is weak but it demonstrates the viscoelastic nature of the hydrogels. The estimated elastic moduli range from 2-3.5 kPa as expected (87). There is an increase in the elastic modulus of the gel with speed; no influence of the maximum applied load below 40nN was detected (not shown).

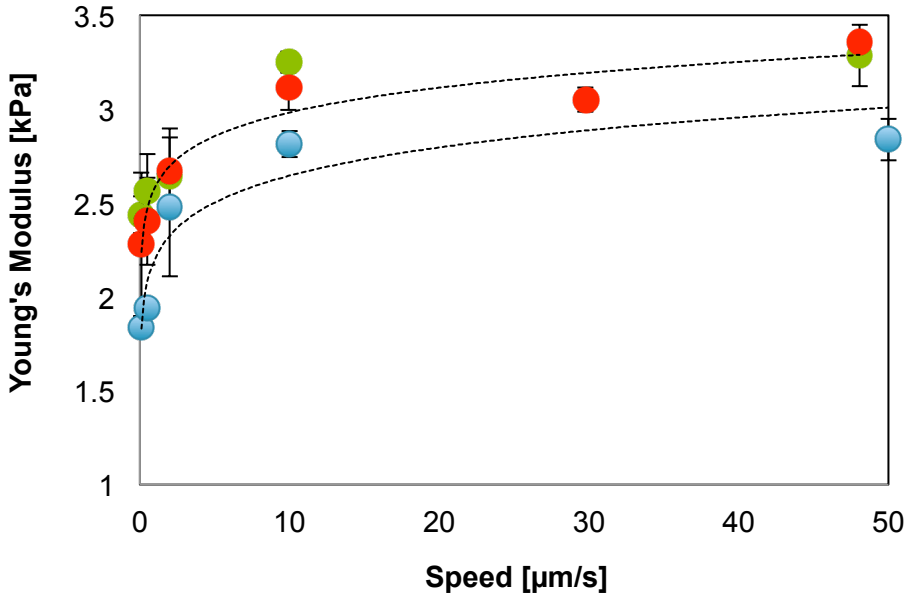

Figure 12: Young modulus as a function of the speed for the PAAm hydrogel (Poisson ratio=0.45) at the maximum load of 40nN. Blue, red and green points hydrogel were 1 day, 1 day and 15 days old, respectively.

Indentation-rate-dependent elastic moduli are characteristic of viscoelastic materials. When polymer films are confined between two surfaces, the time-dependent (or speed-dependent) response can be attributed to different mechanisms, each with a characteristic relaxation time (88). First, solvent has to flow out through or into the network of increasingly compressed gels; second, the coils themselves must reorder as they become compressed or uncompressed.

Alternative time-dependent processes, such as the formation of segment-segment or segment – counter surface interactions can occur, and contribute to the pull off and hysteresis. While desorption of polymers would also lead to a time-dependent response, the reproducibility of the results along the course of each experiment demonstrated the system did not changed. Successive indentation measurements overlap well and lead to a small standard deviation, meaning that there is no delayed or long-term viscoelastic recovery (86). The standard deviation is smaller than discrepancies observed between hydrogels and different positions (see different curves in figure 13).

The results for the PEM adsorbed onto the hydrogel are shown in figure 13. The difference between the elastic moduli of the pure PAAm hydrogels and that of the hydrogel-supported PAH-(PSS-PAH)2 is not statistically significant. The weak viscoelasticity is preserved after adsorption of the polyelectrolyte multilayer.

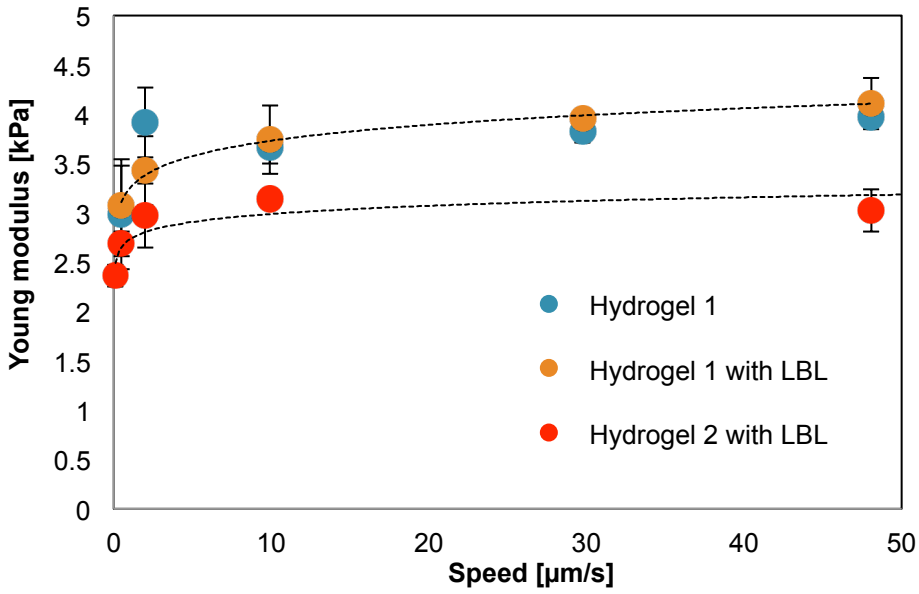

Figure 13: Comparison between the elastic moduli of two PAAm hydrogels after the layer-by-layer formation of PAH-(PSS-PAH)2 with that of the PAAm hydrogel before the layer-by-layer adsorption at a maximum load of 20 nN. Both hydrogel 1 and 2 were 1 day old.

The elastic moduli of the lipid bilayer on a hard silica substrate were determined in preliminary experiments but the experiments failed most likely because of roughness of the colloidal spheres. As the colloidal sphere radius is much larger than the height of the adlayer it is better to determine the elastic modulus with a sharp tip. The elastic modulus is expected to be in the MPa range (89,90), i.e. at least 3 orders of magnitude higher than that of the hydrogel supported polyelectrolyte multilayer. The outlook of this work will be to combine the hydrogel-supported PAH-$(PSS\text{-}PAH)_2$ with the lipid bilayer and determine the resulting Young modulus and viscoelasticity, if present, by colloidal probe normal force measurements.

3.8 Friction measurements

When a load is applied, the colloidal spheres indent the gel, the deformation is large, and thereby the contact area. The contact radius at the normal load of 5 nN is ~1.5 µm assuming the Hertz model. To assure the lateral motion of the gel, the sliding distance needs to be larger than the contact radius. One can identify that the tip is not moving on the shape of the friction loops as demonstrated previously for polymer brushes (91). Thus, the sliding distance in all our experiments was at least 7.5 µm. Figure 14 shows friction vs. applied normal load at constant sliding speed of 3 µm/s for the PAAm hydrogel in water. The good agreement between the measurements at different positions suggests that the gels are homogeneous. Larger differences are obtained between gels synthesized under similar conditions with slightly different ages.

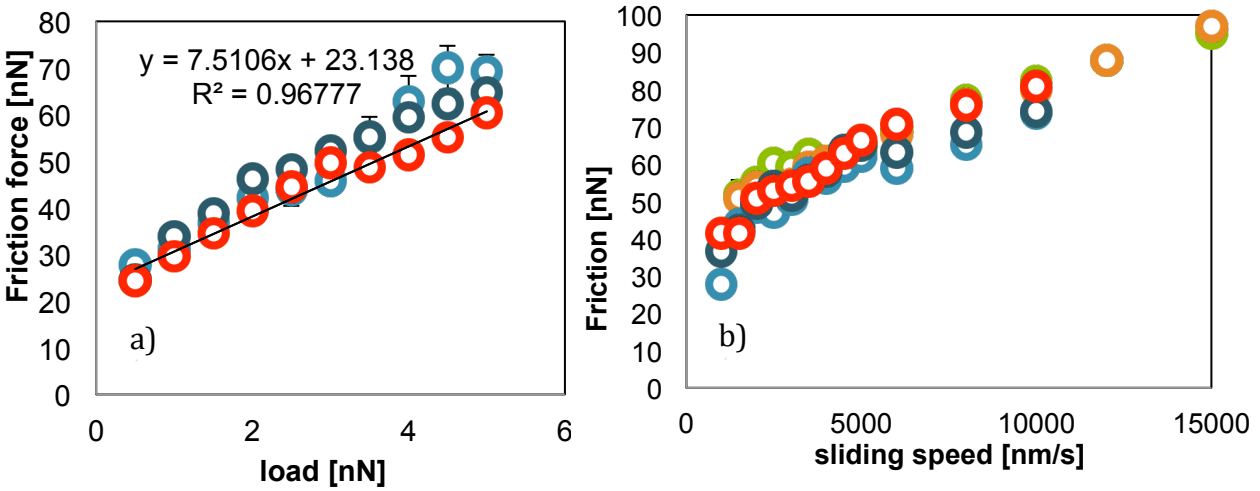

Figure 14: a) Friction vs. load for the PAAm hydrogel at the sliding speed = 3 μm/s, and sliding distance = 15 μm. B) Friction vs. sliding speed at an applied load of 5 nN. The minimum sliding distance is 7.5 μm. Data from 1 and 6 days old hydrogels. Radius of sphere = 6 μm.

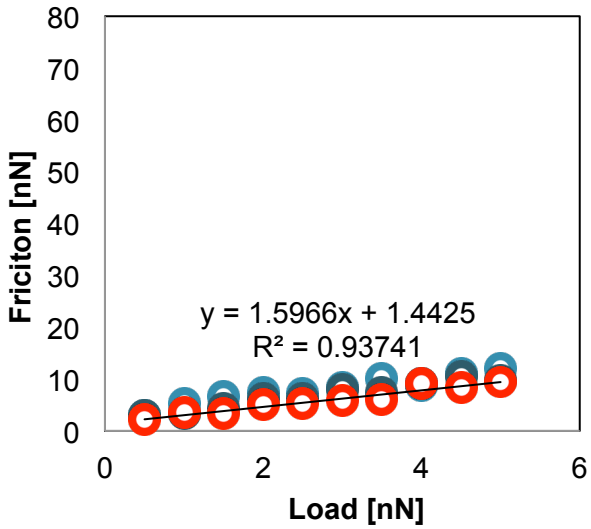

Figure 15: Friction vs. load for the hydrogel-supported PAH-(PSS-PAH)2. Sliding speed = 3 μm/s, sliding distance = 15μm. Radius of sphere = 6 μm. The hydrogel was 1 day old.

Figure 15 shows results for the hydrogel-supported PAH-$(PSS\text{-}PAH)_2$. Interestingly the friction force is reduced by a factor of ~5, although the elastic moduli of hydrogel and hydrogel-supported PEM are similar. This can be explained by the different fluidity of the PEM film compared to the hydrogel. Water can flow through the polymer network in the polyelectrolyte multilayer much easier than through the gel network and this dissipation mechanism aids in reducing friction. This is consistent with our QCM-D results that prove that the hydrogel is much stiffer than the polyelectrolyte multilayer.

Finally, figure 16 shows preliminary results of the friction studies for the silica-supported lipid bilayer. The friction force has not been calibrated, and therefore the values are given in arbitrary units. We expect a different dissipation mechanism for the lipid bilayer as it is only ~ 3nm in thickness, relatively stiff (~20 MPa) and the water content is very low. The very different friction behavior of the lipid bilayer on a hard substrate is demonstrated in figure 16. The load-dependent friction force shows two different regimes, low and high friction regimes, which is usually explained by a change in dissipation mechanism. We hypothesize that in the low friction regime the slip plane is located between the two single lipid monolayers and sliding proceeds with very low interaction between the monolayers. At higher load, stronger interactions between the hydrocarbon chains cause an increase in dissipated energy, as the chains slide past each other, leading to an increase in friction. Another explanation is that the lipid bilayer exhibits a transition from fluid-like to solid-like at higher applied loads and confinement.

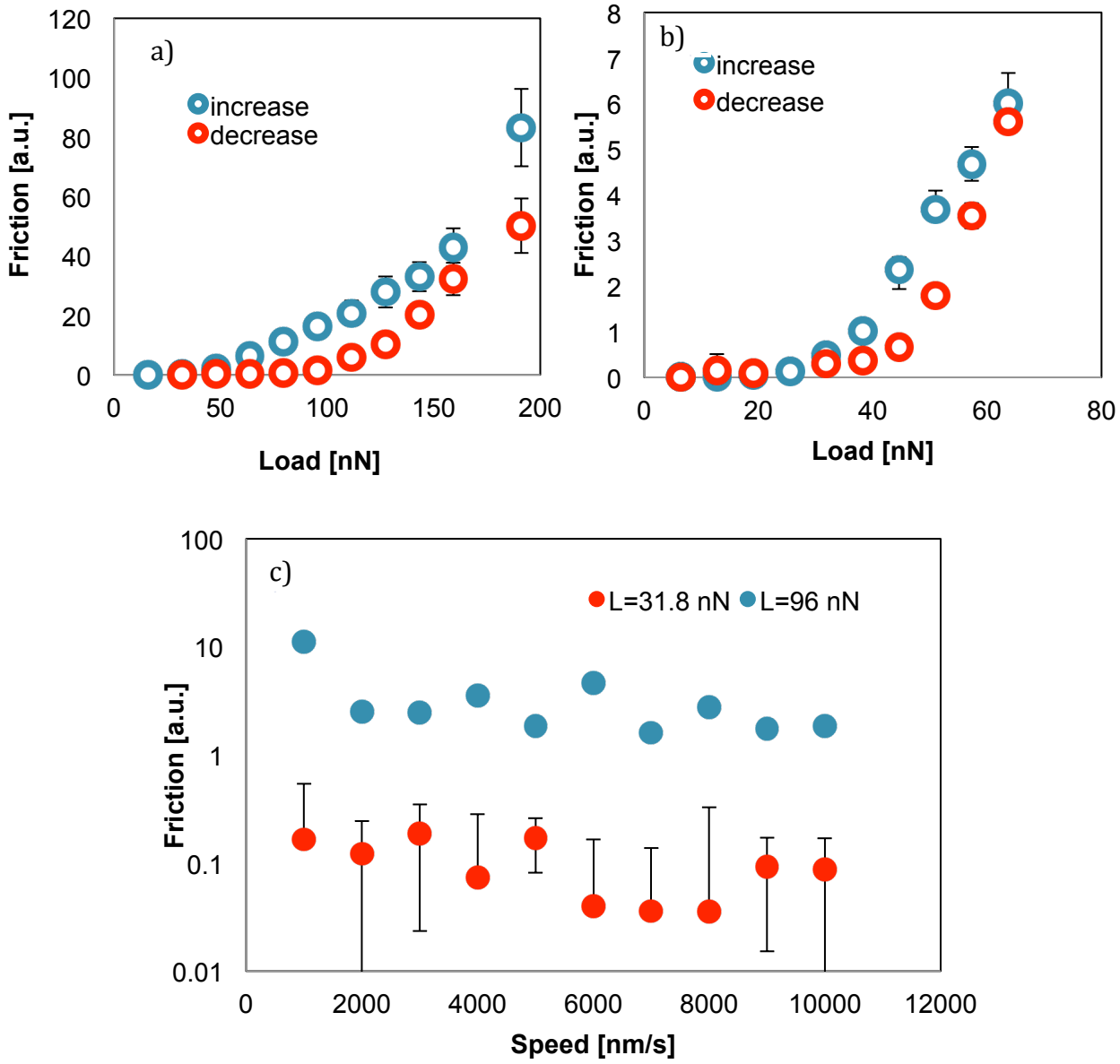

Figure 16: Friction vs. load for the silica-supported lipid bilayer at a maximum load of 200nN (a) and 60 nN (b) and a sliding speed = 5 µm/s, c) Friction vs. speed for the silica-supported lipid bilayer at two different loads: 31.8 nN is still in the low friction regime and 96 nN is in the high friction regime. Minimum sliding distance = 5µm. Radius of sphere = 5µm.

Moreover both diagrams show a hysteresis between friction force upon increase and decrease in load. Thus, there is dissipation of energy or in other words, a change of properties of the lipid bilayer, that is not completely reversible within the time scale of the experiment. This is observed in lipid bilayers at different maximum loads in figures 16a and 16b. The two friction regimes are also pronounced in the friction vs. speed, as shown in figure 16c, where each curve was obtained at a different load. Figure 16 also show that the speed does not induce any relevant change of response of the system. Future work will

include the investigation of the influence of the soft support, i.e. the hydrogel-PEM complex, on the nanomechanics of the lipid bilayer, as well as the influence of the lipid bilayer on the nanomechanics of the hydrogel.

CONCLUSIONS

Studying the interactions between model cells and aqueous environment is applied to investigate cytotoxicity. In contrast to the classical bilayer-solid substrate model, cell membrane model consisting of a polymer-supported lipid-bilayer is a relatively new but very promising approach. The novelty of this work has been to use a hydrogel as the support for the lipid bilayer. Some of the advantages are to provide a longer travel path for particles to diffuse in and to mimic better the mechanical properties of living cells; both of them can be tuned upon selection of proper synthesis parameters. In this project, PAAm hydrogel was selected as the polymer cushion. By adjusting the concentration of monomer and crosslinker, we were able to adjust the PAAm hydrogel to stiffness about 3 kPa, which is similar to that of real cells. It was found that formation of the lipid bilayer on the hydrogel is a very challenging process, likely owing to the strong hydration of the hydrogel. The best approach to promote the adsorption of the lipids on the hydrogel was a layer-by-layer method with alternating cationic and anionic polyelectrolytes. Four to five polyelectrolyte layers consisting of PAH and PSS, positively and negatively charged, respectively, were adsorbed alternatively on PAAm hydrogel and the formation of the PEM was characterized by several techniques. Having PAH as top layer and negatively charged lipid vesicles, the adsorption of lipids on the hydrogel-supported PEM was driven by electrostatic interactions. Adsorption was enhanced by calcium ions in solution which indicates that despite the PAH top layer, there was a high surface density of sulfonate from the layer below. PAH had a much smaller MW than PSS which might be responsible for the excess of sulfonate. It is suggested to test the feasibility of other cationic polymers, with higher MW in future.

It is to note that a charged hydrogel (PAAm-co-IA) as cushion was also studied here but the results were not satisfactory. The charge density within the hydrogel enhanced polyelectrolyte absorption, among others, and a very pronounced collapse and swelling were observed; besides it was very challenging to graft the PAAm-co-IA hydrogel to the substrate; all this made difficult to get high-accuracy QCM data and their evaluation. The use of other charged hydrogels might be an option. This requires further research, which is outside the scope of this work.

Formation of lipid bilayer on silica surface is well known. Lipid vesicles first adsorb as intact vesicles. When the substrate is covered by a certain amount of lipid vesicles, they rupture and fuse into a bilayer. The successful formation of a lipid bilayer was demonstrated by QCM-D measurements and the full coverage of the silica-coated QCM sensor was confirmed by AFM imaging. These results were compared to the kinetics of adsorption of the lipid bilayer on a hydrogel-supported PEM. Although the frequency did only continuously decrease, the small peak in dissipation supported the formation of the lipid bilayer on the hydrogel-PEM complexes. Albumin adsorption was consistent with a partial coverage

of the hydrogel-supported PEM with a lipid bilayer. AFM imaging of the PAAm hydrogel-PEM complexes after lipid adsorption will be performed in close future to fully verify the formation of the lipid bilayer. These measurements are very challenging, as they imply imaging soft matter in liquid medium.

AFM nanoindentation and lateral force microscopy were performed to investigate the mechanical properties of different systems: (a) PAAm hydrogel, (b) PAAm hydrogel-supported PEM, and (c) lipid bilayer. The viscoelastic behavior of the PAAm hydrogel and hydrogel-supported PEM was demonstrated by the slight increase of the Young modulus with the indentation rate at relatively high loads (20- 40 nN). This result indicates that hydrogel mimic better the viscoelastic behavior of cells, than polymer films of a few nanometers do. The friction between the colloidal sphere and hydrogel increased with applied load. This is usually caused by a dehydration of the system, which enhances interactions between the polymer chains. The increase in friction with speed is explained by an increase in the number of physical bonds that form with time with increase in speed. The agreement between measurements taken at different spots on PAAm hydrogel suggests that the gels are homogenous. While the elastic modulus of hydrogel-PEM complexes is similar to that of the PAAm hydrogel, the response upon shear was very different. Preliminary results show that the presence of the PEM layer strongly reduces friction force, most likely because of the high fluidity of this layer compared to the gel. The fluidity of the hydrogel is much lower, despite the large amount of water, most likely caused by the complex pore network that difficult the flow of water, while it is easier within the PEM . For the lipid bilayer on a silica support low and high friction regimes were identified, perhaps owing to a transition from fluid-like to solid-like of the lipid bilayer induced by the applied load, The question that remains to be answered is the mechanical behavior resulting from the combination of the hydrogel-supported PEM and the lipid bilayer. For that purpose, nanoindentation and lateral force microscopy measurements will be performed with both sharp tip and silica microsphere on the hydrogel-supported PEM after lipid adsorption in close future.

The proposed novel model cell is expected to mimic the nanomechanic behavior of cells with more accuracy than other existent model systems to date. This soft composite can simulate the mechanical response of cells of living organisms, and therefore a fundamental understanding of the nanomechanics under different conditions will be of extreme value.. The hydrogel properties (e.g. stiffness, pore size) can be tuned, as long as it allows the formation of a polyelectrolyte multilayer for the lipid adsorption. Decoration of this lipid bilayer with proteins and polysaccharides should be also possible, and therefore it offers a great flexibility in the design of model systems. It is also expected that this system will be applied to investigate the interactions with the aqueous environment, e.g. with nanoparticles, ions, heavy metals, virus, proteins, etc. as a platform to investigate cytotoxicity.

REFERENCES

1. Valles, E., et al. "Equilibrium swelling and mechanical properties of hydrogels of acrylamide and itaconic acid or its esters." *Polymer bulletin* 44.1 (2000): 109-114.
2. Tanaka, Toyoichi, et al. "Phase transitions in ionic gels." *Physical Review Letters* 45.20 (1980): 1636.
3. Tanaka, Toyoichi. "Collapse of gels and the critical endpoint." *Physical Review Letters* 40.12 (1978): 820.
4. Nohava, Jiri, Michael Swain, and Philipp Eberwein. "Micromechanical Properties of Polyacrylamide Hydrogels Measured by Spherical Nanoindentation." *Key Engineering Materials* 606 (2014): 121-124.
5. Qiu, Yong, and Kinam Park. "Environment-sensitive hydrogels for drug delivery." *Advanced drug delivery reviews* 64 (2012): 49-60.
6. Hyon, Suong-Hyu, et al. "Poly (vinyl alcohol) hydrogels as soft contact lens material." *Journal of Biomaterials Science, Polymer Edition* 5.5 (1994): 397-406.
7. Noguchi, Takashi, et al. "Poly (vinyl alcohol) hydrogel as an artificial articular cartilage: evaluation of biocompatibility." *Journal of Applied Biomaterials* 2.2 (1991): 101-107.
8. Kayaman, Nilhan, et al. "Interpenetrating hydrogel networks based on polyacrylamide and poly (itaconic acid): synthesis and characterization."*Macromolecular Chemistry and Physics* 200.1 (1999): 231-238.
9. Nel, Andre E., et al. "Understanding biophysicochemical interactions at the nano–bio interface." *Nature materials* 8.7 (2009): 543-557.
10. Beney, L., and P. Gervais. "Influence of the fluidity of the membrane on the response of microorganisms to environmental stresses." *Applied microbiology and biotechnology* 57.1-2 (2001): 34-42.
11. Tamm, Lukas K., and Harden M. McConnell. "Supported phospholipid bilayers."*Biophysical journal* 47.1 (1985): 105.
12. Merkel, R., E. Sackmann, and E. Evans. "Molecular friction and epitactic coupling between monolayers in supported bilayers." *Journal de Physique*50.12 (1989): 1535-1555.
13. McConnell, H. M., et al. "Supported planar membranes in studies of cell-cell recognition in the immune system." *Biochimica et Biophysica Acta (BBA)-Reviews on Biomembranes* 864.1 (1986): 95-106.
14. Naumann, Christoph A., et al. "The polymer-supported phospholipid bilayer: tethering as a new approach to substrate-membrane stabilization."*Biomacromolecules* 3.1 (2002): 27-35.
15. Schmitt, Johannes, Birgit Danner, and Thomas M. Bayerl. "Polymer cushions in supported phospholipid bilayers reduce significantly the frictional drag between bilayer and solid surface." *Langmuir* 17.1 (2001): 244-246.
16. Sackmann, Erich. "Supported membranes: scientific and practical applications." *Science* 271.5245 (1996): 43-48.
17. Tanaka, Motomu, and Erich Sackmann. "Polymer-supported membranes as models of the cell surface." *Nature* 437.7059 (2005): 656-663.
18. Chen, Kai Loon, and Geoffrey D. Bothun. "Nanoparticles meet cell membranes: probing nonspecific interactions using model membranes." *Environmental science & technology* 48.2 (2013): 873-880.
19. Nel, Andre E., et al. "Understanding biophysicochemical interactions at the nano–bio interface." *Nature materials* 8.7 (2009): 543-557.
20. Xiao, Xiaoyin, et al. "Surface charge dependent nanoparticle disruption and deposition of lipid bilayer assemblies." *Langmuir* 28.50 (2012): 17396-17403.
21. Chithrani, B. Devika, Arezou A. Ghazani, and Warren CW Chan. "Determining the size and shape dependence of gold nanoparticle uptake into mammalian cells." *Nano letters* 6.4 (2006): 662-668.
22. R. Shukla, V. Bansal, M. Chaudhary, A. Basu, R. R. Bhonde, M. Sastry, Langmuir 2005, 21, 10644.

23. Ma, Yong-Jie, and Hong-Chen Gu. "Study on the endocytosis and the internalization mechanism of aminosilane-coated Fe3O4 nanoparticles in vitro."*Journal of Materials Science: Materials in Medicine* 18.11 (2007): 2145-2149.
24. Marra, Johan, and Jacob Israelachvili. "Direct measurements of forces between phosphatidylcholine and phosphatidylethanolamine bilayers in aqueous electrolyte solutions." *Biochemistry* 24.17 (1985): 4608-4618.
25. Dagastine, Raymond R., et al. "Dynamic forces between two deformable oil droplets in water." *Science* 313.5784 (2006): 210-213.
26. McClellan, Scott J., and Elias I. Franses. "Adsorption of bovine serum albumin at solid/aqueous interfaces." *Colloids and Surfaces A: Physicochemical and Engineering Aspects* 260.1 (2005): 265-275.
27. Norde, Willem. "Driving forces for protein adsorption at solid surfaces." *Macromolecular Symposia*. Vol. 103. No. 1. Hüthig & Wepf Verlag, 1996.
28. Jeon, Joong S., Srini Raghavan, and R. P. Sperline. "Quantitative analysis of albumin adsorption onto uncoated and poly (ether) urethane-coated ZnSe surfaces using the attenuated total reflection FTIR technique." *Colloids and Surfaces A: Physicochemical and Engineering Aspects* 92.3 (1994): 255-265.
29. Kim, Joonyeong, and Gabor A. Somorjai. "Molecular packing of lysozyme, fibrinogen, and bovine serum albumin on hydrophilic and hydrophobic surfaces studied by infrared-visible sum frequency generation and fluorescence microscopy." *Journal of the American Chemical Society* 125.10 (2003): 3150-3158.
30. Zhang, Miqin, Tejal Desai, and Mauro Ferrari. "Proteins and cells on PEG immobilized silicon surfaces." *Biomaterials* 19.10 (1998): 953-960.
31. Giacomelli, Carla E., Maria GEG Bremer, and Willem Norde. "ATR-FTIR study of IgG adsorbed on different silica surfaces." *Journal of colloid and interface science* 220.1 (1999): 13-23.
32. Vermette, Patrick, et al. "Albumin and fibrinogen adsorption onto phosphatidylcholine monolayers investigated by Fourier transform infrared spectroscopy." *Colloids and Surfaces B: Biointerfaces* 29.4 (2003): 285-295.
33. Norde, W., and J. Lyklema. "The adsorption of human plasma albumin and bovine pancreas ribonuclease at negatively charged polystyrene surfaces: I. Adsorption isotherms. Effects of charge, ionic strength, and temperature."*Journal of Colloid and Interface Science* 66.2 (1978): 257-265.
34. Van Dulm, P., W. Norde, and J. Lyklema. "Ion participation in protein adsorption at solid surfaces." *Journal of Colloid and Interface Science* 82.1 (1981): 77-82.
35. Bao, Gang, and S. Suresh. "Cell and molecular mechanics of biological materials." *Nature materials* 2.11 (2003): 715-725.
36. Yeung, Tony, et al. "Effects of substrate stiffness on cell morphology, cytoskeletal structure, and adhesion." *Cell motility and the cytoskeleton* 60.1 (2005): 24-34.
37. Zemel, A., et al. "Optimal matrix rigidity for stress-fibre polarization in stem cells." *Nature physics* 6.6 (2010): 468-473.
38. Clark, Andrew G., and Ewa Paluch. "Mechanics and regulation of cell shape during the cell cycle." *Cell cycle in development*. Springer Berlin Heidelberg, 2011. 31-73.
39. Collinsworth, Amy M., et al. "Apparent elastic modulus and hysteresis of skeletal muscle cells throughout differentiation." *American Journal of Physiology-Cell Physiology* 283.4 (2002): C1219-C1227.
40. Stoimenov, Peter K., et al. "Metal oxide nanoparticles as bactericidal agents. "*Langmuir* 18.17 (2002): 6679-6686.
41. Guck, Jochen, et al. "Optical deformability as an inherent cell marker for testing malignant transformation and metastatic competence." *Biophysical journal* 88.5 (2005): 3689-3698.
42. Lekka, M., et al. "Elasticity of normal and cancerous human bladder cells studied by scanning force microscopy." *European Biophysics Journal* 28.4 (1999): 312-316.
43. Janmey, Paul A., and Christopher A. McCulloch. "Cell mechanics: integrating cell responses to mechanical stimuli." *Annu. Rev. Biomed. Eng.* 9 (2007): 1-34.

44. Fabry, Ben, et al. "Scaling the microrheology of living cells." *Physical review letters* 87.14 (2001): 148102.
45. Puig-De-Morales, Marina, et al. "Measurement of cell microrheology by magnetic twisting cytometry with frequency domain demodulation." *Journal of Applied Physiology* 91.3 (2001): 1152-1159.
46. Fernández, Pablo, Pramod A. Pullarkat, and Albrecht Ott. "A master relation defines the nonlinear viscoelasticity of single fibroblasts." *Biophysical journal*90.10 (2006): 3796-3805.
47. Li, Q. S., et al. "AFM indentation study of breast cancer cells." *Biochemical and biophysical research communications* 374.4 (2008): 609-613.
48. Docheva, Denitsa, et al. "Researching into the cellular shape, volume and elasticity of mesenchymal stem cells, osteoblasts and osteosarcoma cells by atomic force microscopy." *Journal of cellular and molecular medicine* 12.2 (2008): 537-552.
49. Nawaz, Schanila, et al. "Cell visco-elasticity measured with AFM and optical trapping at sub-micrometer deformations." *PLoS One* 7.9 (2012): e45297.
50. Ladjal, Hamid, et al. "Atomic force microscopy-based single-cell indentation: Experimentation and finite element simulation." *Intelligent Robots and Systems, 2009. IROS 2009. IEEE/RSJ International Conference on*. IEEE, 2009.
51. Alcaraz, Jordi, et al. "Microrheology of human lung epithelial cells measured by atomic force microscopy." *Biophysical journal* 84.3 (2003): 2071-2079.
52. Tse, Justin R., and Adam J. Engler. "Preparation of hydrogel substrates with tunable mechanical properties." *Current protocols in cell biology* (2010): 10-16.
53. Rault, J., et al. "Thermal transitions in hydrogels of poly (ethyl acrylate)/poly (hydroxyethyl acrylate) interpenetrating networks." *Macromolecules* 30.25 (1997): 7866-
By adjusting the amount of cross-linker and amount of monomer, the mechanical properties of hydrogels can be altered.7873.
54. Rault, J., et al. "Thermal transitions in hydrogels of poly (ethyl acrylate)/poly (hydroxyethyl acrylate) interpenetrating networks." *Macromolecules* 30.25 (1997): 7866-7873.
55. Bera, Rabin, Ayan Dey, and Debabrata Chakrabarty. "." *Polymer Engineering & Science* 55.1 (2015): 113-122.
56. Keller, C. A., and B. Kasemo. "Surface specific kinetics of lipid vesicle adsorption measured with a quartz crystal microbalance." *Biophysical journal*75.3 (1998): 1397-1402.
57. Heuberger, Manfred, and Tobias E. Balmer. "The transmission interferometric adsorption sensor." *Journal of Physics D: Applied Physics* 40.23 (2007): 7245.
58. Rico, Félix, et al. "Probing mechanical properties of living cells by atomic force microscopy with blunted pyramidal cantilever tips." *Physical Review E* 72.2 (2005): 021914.
59. Hutter, Jeffrey L., and John Bechhoefer. "Calibration of atomic-force microscope tips." *Review of Scientific Instruments* 64.7 (1993): 1868-1873.
60. Radmacher, Manfred, et al. "Measuring the viscoelastic properties of human platelets with the atomic force microscope." *Biophysical journal* 70.1 (1996): 556-567.
61. Ogletree, D. F., Robert W. Carpick, and Miguel Salmeron. "Calibration of frictional forces in atomic force microscopy." *Review of Scientific Instruments*67.9 (1996): 3298-3306.
62. Hooper, Herbert H., et al. "Swelling equilibria for positively ionized polyacrylamide hydrogels." *Macromolecules* 23.4 (1990): 1096-1104.
63. Fujii, Akihiro, et al. "pH-responsive behavior of hydrogel microspheres altered by layer-by-layer assembly of polyelectrolytes." *Colloids and Surfaces A: Physicochemical and Engineering Aspects* 337.1 (2009): 159-163.
64. Wong, John E., and Walter Richtering. "Surface modification of thermoresponsive microgels via layer-by-layer assembly of polyelectrolyte multilayers." *Smart Colloidal Materials*. Springer Berlin Heidelberg, 2006. 45-51.
65. Wong, John E., et al. "Direct evidence of layer-by-layer assembly of polyelectrolyte multilayers on soft and porous temperature-sensitive PNiPAM microgel using fluorescence correlation spectroscopy." *The Journal of Physical Chemistry B* 111.29 (2007): 8527-8531.

66. De Geest, B. G., et al. "Layer-by-layer coating of degradable microgels for pulsed drug delivery." *Journal of controlled release* 116.2 (2006): 159-169.
67. Holmes, Diana L., and Nancy C. Stellwagen. "Estimation of polyacrylamide gel pore size from Ferguson plots of linear DNA fragments. II. Comparison of gels with different crosslinker concentrations, added agarose and added linear polyacrylamide." *Electrophoresis* 12.9 (1991): 612-619.
68. Tao, Yong, and Yu-Mei Qin. "Effect of Solute-Polymer Interactions on Sorption and Diffusion in Polyacrylamide Gels." *Journal of Macromolecular Science, Part B: Physics* 46.5 (2007): 915-929.
69. Serizawa, Takeshi, et al. "Polyelectrolyte multilayers prepared on hydrogel surfaces." *Journal of Polymer Science Part A: Polymer Chemistry* 43.5 (2005): 1062-1067.
70. Yamanlar, Seda, et al. "Surface functionalization of hyaluronic acid hydrogels by polyelectrolyte multilayer films." *Biomaterials* 32.24 (2011): 5590-5599.
71. Shin, Yongjin, et al. "Insights into hydrophobic molecule release from polyelectrolyte multilayer films using in situ and ex situ techniques." *Physical Chemistry Chemical Physics* 16.40 (2014): 22409-22417.
72. Nalam, Prathima C., et al. "Two-Fluid Model for the Interpretation of Quartz Crystal Microbalance Response: Tuning Properties of Polymer Brushes with Solvent Mixtures." *The Journal of Physical Chemistry C* 117.9 (2013): 4533-4543.
73. Heuberger, Manfred, and Tobias E. Balmer. "The transmission interferometric adsorption sensor." *Journal of Physics D: Applied Physics* 40.23 (2007): 7245.
74. Sannomiya, Takumi, et al. "Simultaneous refractive index and thickness measurement with the transmission interferometric adsorption sensor." *Journal of Physics D: Applied Physics* 43.40 (2010): 405302.
75. Chen, Jiangshan, et al. "Asymmetric lipid bilayer sandwiched in polyelectrolyte multilayer films through layer-by-layer assembly." *Soft matter* 5.1 (2009): 228-233.
76. Fischlechner, Martin, et al. "Lipid layers on polyelectrolyte multilayer supports."*Soft Matter* 4.11 (2008): 2245-2258.
77. Richter, Ralf P., Rémi Bérat, and Alain R. Brisson. "Formation of solid-supported lipid bilayers: an integrated view." *Langmuir* 22.8 (2006): 3497-3505.
78. Schönhoff, Monika. "Layered polyelectrolyte complexes: physics of formation and molecular properties." *Journal of Physics: Condensed Matter* 15.49 (2003): R1781.
79. Hardy, Gregory J., Rahul Nayak, and Stefan Zauscher. "Model cell membranes: Techniques to form complex biomimetic supported lipid bilayers via vesicle fusion." *Current opinion in colloid & interface science* 18.5 (2013): 448-458.
80. Chiem, Linh T., et al. "An in situ ATR–FTIR study of polyacrylamide adsorption at the talc surface." *Journal of colloid and interface science* 297.1 (2006): 54-61.
81. Wang, Zhaoyi, et al. "Microfluidic studies of polymer adsorption in flow." *Lab on a Chip* 15.9 (2015): 2110-2116.
82. Cornejo, Jay Jesus Molino, Eitaro Matsuoka, and Hirofumi Daiguji. "Size control of hollow poly-allylamine hydrochloride/poly-sodium styrene sulfonate microcapsules using the bubble template method." *Soft Matter* 7.5 (2011): 1897-1902.
83. Ladam, Guy, et al. "Protein interactions with polyelectrolyte multilayers: interactions between human serum albumin and polystyrene sulfonate/polyallylamine multilayers." *Biomacromolecules* 1.4 (2000): 674-687.
84. Sneddon, Ian N. "The relation between load and penetration in the axisymmetric Boussinesq problem for a punch of arbitrary profile." *International Journal of Engineering Science* 3.1 (1965): 47-57.
85. Tranchida, Da, et al. "Nanoscale mechanical characterization of polymers by atomic force microscopy (AFM) nanoindentations: viscoelastic characterization of a model material." *Measurement Science and Technology* 20.9 (2009): 095702.
86. Tranchida, Davide, Stefano Piccarolo, and Maria Soliman. "Nanoscale mechanical characterization of polymers by AFM nanoindentations: critical approach to the elastic characterization." *Macromolecules* 39.13 (2006): 4547-4556.

87. Tse, Justin R., and Adam J. Engler. "Preparation of hydrogel substrates with tunable mechanical properties." *Current protocols in cell biology* (2010): 10-16.
88. Israelachvili, J. N., *Intermolecular and Surface Forces: Revised Third Edition*. Elsevier Science: 2011.
89. Canale, C., et al. "Force spectroscopy as a tool to investigate the properties of supported lipid membranes." *Microscopy research and technique* 73.10 (2010): 965-972.
90. Dante, Silvia, et al. "Nanoscale structural and mechanical effects of beta-amyloid (1–42) on polymer cushioned membranes: A combined study by neutron reflectometry and AFM Force Spectroscopy." *Biochimica et Biophysica Acta (BBA)-Biomembranes* 1808.11 (2011): 2646-2655.
91. Li, Ang, et al. "Stratified Polymer Grafts: Synthesis and Characterization of Layered 'Brush'and 'Gel'Structures." *Advanced Materials Interfaces* 1.1 (2014).

APPENDIX: SUPPLEMENTARY INFORMATION

A1. QMC results for a stiffer hydrogel

It has been reported that hydrogels age and become stiffer with time after synthesis. We have observed that 1-day old hydrogels were slightly stiffer than fresh made hydrogels, and this influenced the collapse/swelling behavior significantly in the adsorption measurements. The decrease in dissipation during the adsorption of the 1st layer of PSS on 1d-hydrogel was reduced, as shown in Figure SM1 b). The subsequent adsorption results are consistent with the results obtained for fresh hydrogels (Figure SM1 a). The results of QCM and TInAS experiments discussed in this thesis correspond to freshly prepared gels.

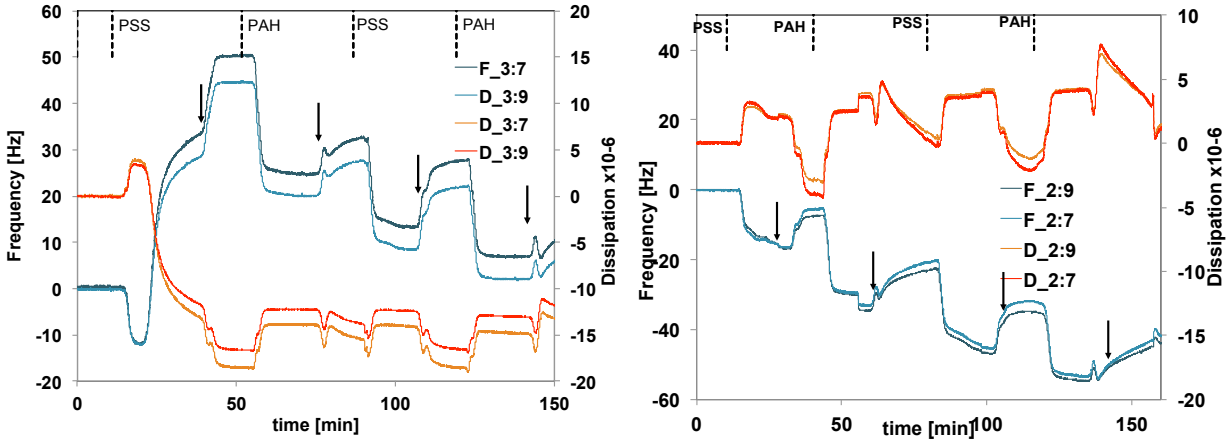

Figure 17: QCM-D data (frequency and dissipation) for the formation of $(PSS\text{-}PAH)_2$ on two PAAm hydrogels: a) freshly prepared and b) 1 day old.

A2. Lipid vesicles formation on silica sensor

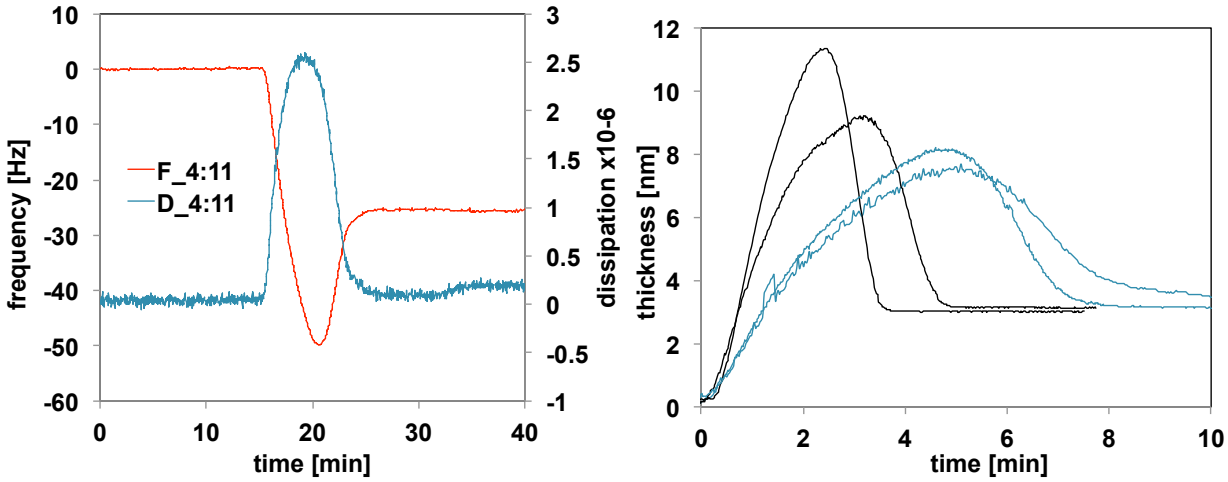

Figure 18: Left) Representative changes in frequency and dissipation (11th overtone), and right) Adlayer thickness calculated with the Voigt model, during vesicle adsorption and lipid bilayer formation on a silica substrate. The different kinetics results from the different vesicle radius (32 nm in blue and 130 nm in black). Once the vesicle surface coverage reaches a critical concentration, the vesicles spontaneously rupture and fuse to form a continuous lipid bilayer. The frequency increase is due to lipid bilayer displacement of adsorbed vesicles and the buffer released from within the vesicle interior. A complete bilayer is characterized by a dip in Δf and peak ΔD with time, resulting in a final Δf of ~–26 Hz and a ΔD of ~0.2*10^(-6). Assumed density for the lipid bilayer = 1.5 g/cm^3.

A3. Albumin adsorption on PAAm hydrogels

Sorption of a model protein, bovine serum albumin (BSA), was also studied on the porous PAAm hydrogels. Albumin can diffuse into the gel and absorb within the pores (absorption), and also adsorb at the hydrogel/fluid interface (adsorption). QCM and TInAS did not show similar sorption kinetics but the final adlayer thickness was similar (~3.5 nm). This is ~2x the optical thickness of albumin on a bare silica substrate, which demonstrates the larger surface area of the hydrogel owing to the porosity and to surface roughness). The origin for the discrepancy of the kinetics lies in the measuring principle, as described below.

In the QCM experiments, the sorption kinetics is initially very fast and after ~2 minutes, the increase in adlayer thickness is slow, most likely caused by a small diffusion of BSA into the hydrogel. After ~90 minutes the solvent (hepes) is injected into the cell to remove weakly adsorbed albumin but the mass remained constant.

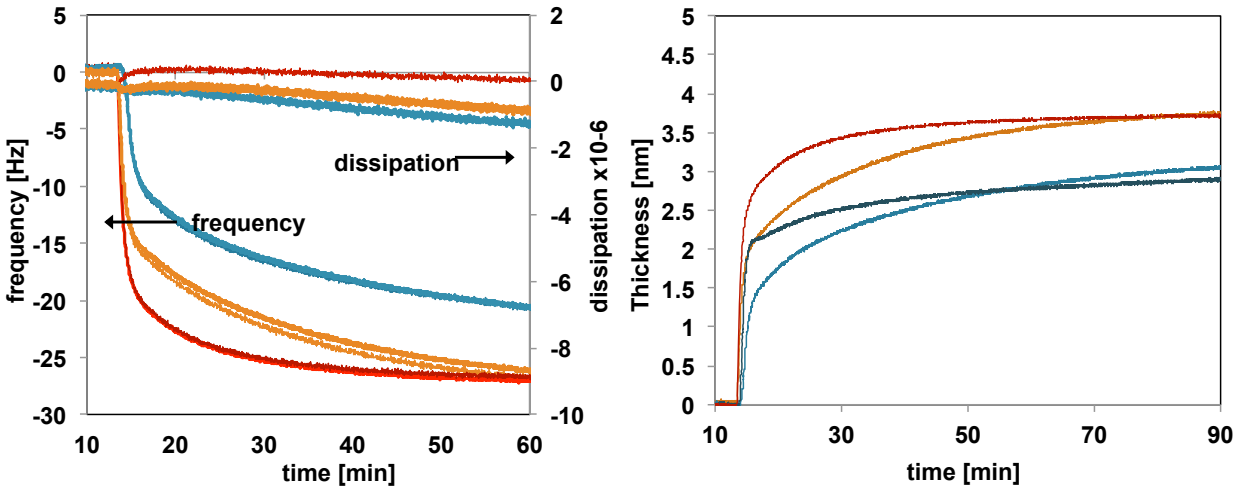

Figure 19: Left) Change of frequency and of dissipation (x10^{-6}) for the 7th overtone during sorption of albumin in 10 mM hepes on freshly prepared PAAm hydrogels. The Voigt model was not used owing to the negative dissipation that results from the diffusion of albumin into the gel. Results from three measurements on different gels (freshly prepared) are shown here. Right) Adlayer thickness of albumin calculated with the Sauerbrey equation (density = 1.32 g/cm3). The synthesized gels vary in their properties as shown in the different kinetics. The thickness of the gels in QCM experiments is ~4 µm.

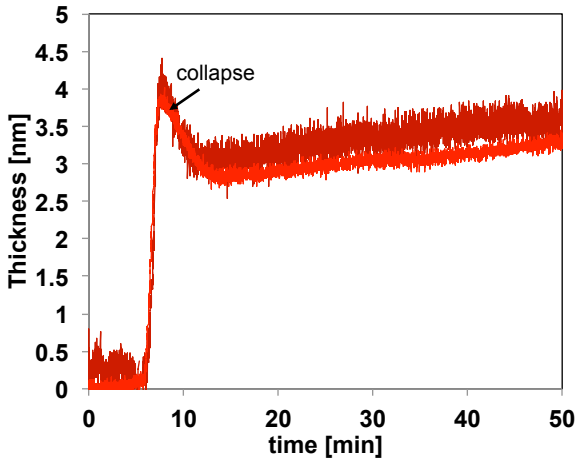

Figure 20: Optical thickness of the albumin adlayer during sorption onto PAAm hydrogel in hepes 10 mM, assuming a constant refractive index of n=1.42 for albumin and n=1.35 for the gel. There is a collapse after the initial adsorption caused by a osmotic pressure gradient: upon albumin sorption, the hydrogel becomes effectively charged. The collapse of the gel brings the system to the new equilibrium swelling state. The dry thickness of the gels in TInAS experiments is ~187±9 nm, and the real thickness ~6 µm.

TInAS measurements showed an initial increase of the optical thickness, followed by a decrease, and a final gradual increase under similar conditions to the QCM experiments. We explain this trend through the superposition of adsorption and collapse of the hydrogel. TInAS is not sensitive to the loss of water, but the collapse leads to an increase in refractive index, thus, to a change in the optical path $\Delta(Tn)$. As we

assume the refractive index of the gel to remain constant, the adlayer optical thickness decreases. Such collapse was also clear in QCM experiments as the dissipation became negative, indicating that the substrate became stiffer. The collapse of the hydrogel after albumin sorption is caused by a gradient in osmotic pressure. Although the hydrogel PAAm is neutral and therefore not sensitive to changes in ionic strength, upon albumin sorption the hydrogel becomes "effectively charged" and thereby it responds to the electrolyte concentration in the solution. To further demonstrate this, the response of the hydrogel after albumin sorption to changes in ionic strength was also investigated.

A4. Collapse and swelling behavior of hydrogels-albumin complexes owing to osmotic pressure gradients

The sorption of albumin in water differs from that in Hepes, as shown in figure 5. Upon rinsing the hydrogel–albumin complex with water, an increase in optical thickness is observed (swelling) to eliminate the gradient in osmotic pressure –the high charge density within the gel-albumin complex is reduced by an increase in volume. In both systems, a decrease in optical thickness (collapse) occurred when the hydrogel-albumin complexes were exposed to $CaCl_2$ solution, owing to smaller charge density within the gel compared to the solution. In contrast, no collapse of the hydrogel was observed in $CaCl_2$ solutions at a concentration of 1M.

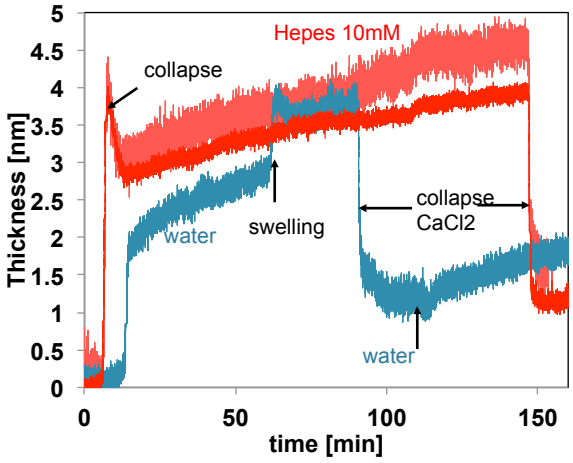

Figure 21: Measured optical thickness of two PAAm gels in hepes 10 mM (red) and in water (blue) during a) absorption of albumin, b) rinsing with the corresponding solvent (time=60 min, hepes and water, respectively), and c) gel collapse when exposed to $CaCl_2$ 1M.

A5. Layer-by-layer formation on silica substrates

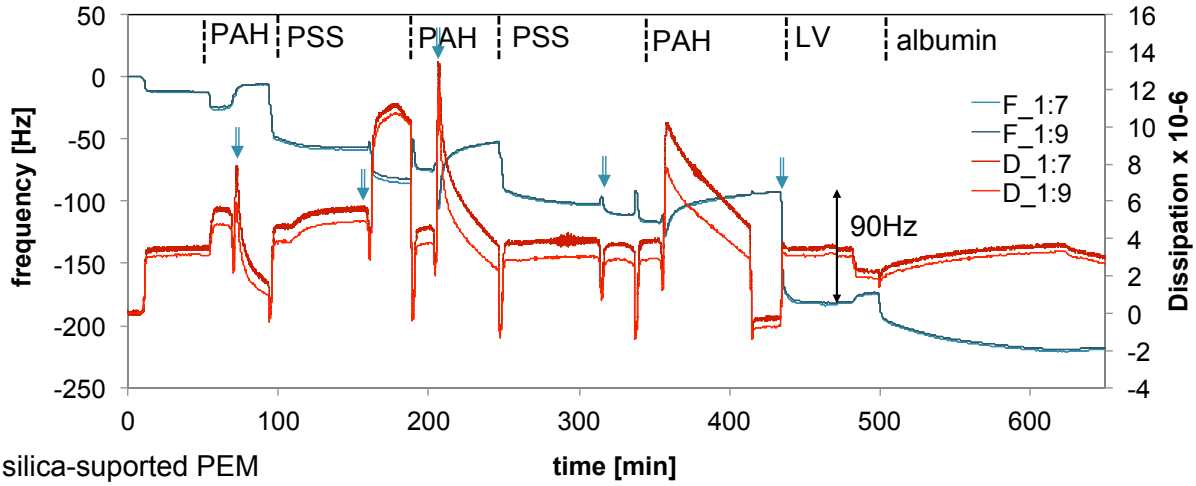

Figure 22: QCM-D data of frequency and dissipation (7th and 9th overtones) during PEM formation on a silica support; the cell was initially rinsed with NaCl solution (500 mM) before flowing polymer solution, which lead to a decrease in frequency and increase in dissipation. The changes of dissipation upon rinsing PAH and PSS are complex owing to the rearrangement of the polymer chains at the interface upon adsorption. There is a strong increase in frequency upon PAH adsorption, which can be induced by partial desorption of PSS and loss of water. This is not observed during the layer-by-layer formation on a hydrogel, demonstrating the significant influence of the support on the PEM structure.

A6. AFM imaging of lipid vesicles on a rough TInAS sensor

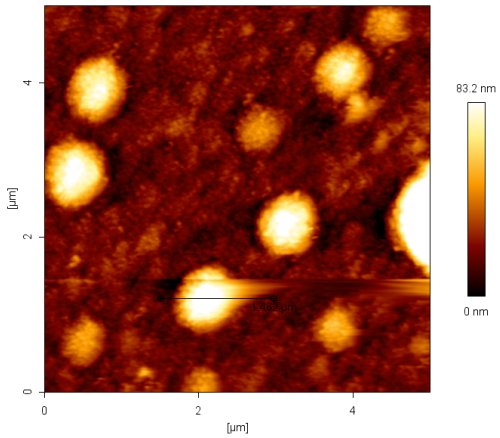

Figure 23: AFM image (contact mode) set point = 1nN of vesicles on a TInAS (Silica) sensor. Sharp tip HQ:CSC38/No Al The lipid bilayer cannot be imaged due to the high roughness of the surface. The vesicles have a size of ~80 nm. Number density = 10 in 25 μm^2